

Lattice QCD Determination of the Bjorken- x Dependence of PDFs at Next-to-next-to-leading Order

Xiang Gao,^{1,*} Andrew D. Hanlon,² Swagato Mukherjee,² Peter Petreczky,² Philipp Scior,² Sergey Syritsyn,^{3,4} and Yong Zhao^{5,†}

¹*Key Laboratory of Quark & Lepton Physics (MOE) and Institute of Particle Physics, Central China Normal University, Wuhan 430079, China*

²*Physics Department, Brookhaven National Laboratory, Bldg. 510A, Upton, New York 11973, USA*

³*RIKEN-BNL Research Center, Brookhaven National Laboratory, Upton, New York 11973*

⁴*Department of Physics and Astronomy, Stony Brook University, Stony Brook, New York 11790*

⁵*Physics Division, Argonne National Laboratory, Lemont, IL 60439, USA*

We develop a procedure to renormalize the quasi parton distribution in the recently proposed hybrid scheme, which features a Wilson-line mass subtraction at large distance in coordinate space, and match it to the $\overline{\text{MS}}$ scheme light-cone parton distribution at next-to-next-to-leading order in perturbation theory. For the first time we apply this procedure to the calculation of pion valence quark distribution using two fine lattices with spacing $a = 0.04$ fm and 0.06 fm and valence pion mass $m_\pi = 300$ MeV, at boost momentum as large as 2.42 GeV. We demonstrate that perturbative matching in the Bjorken- x space yields reliable determination of the valence quark distribution for $0.03 \lesssim x \lesssim 0.80$ with 5–20% uncertainty.

Understanding the inner structure of the proton and other hadrons remains one of the top fundamental questions in nuclear and particle physics nowadays. The parton distribution functions (PDFs), which describe 1D momentum densities of quarks and gluons in a hadron, are the simplest and most important quantities that have been extensively measured from global high-energy scattering experiments and will be probed at unprecedented precision at the future Electron-Ion Collider [1, 2]. Besides the experimental efforts, the first-principles calculations of PDFs using lattice quantum chromodynamics (QCD) are also expected to provide useful predictions.

Computation of the PDFs on a Euclidean lattice has been extremely difficult because they are defined from light-cone correlations with real-time dependence in Minkowski space. For a long time only the lowest few moments of the PDFs were calculable as they are matrix elements of local gauge-invariant operators. Less than a decade ago, a breakthrough was made by large-momentum effective theory (LaMET) [3–5], which starts from a Euclidean “quasi-PDF” (qPDF) in a boosted hadron and calculates the PDF through a large-momentum expansion and perturbative matching of the qPDF in the Bjorken- x (the longitudinal momentum fraction) space. Over the past years, LaMET has led to much progress in the calculations of PDFs and other parton physics [5, 6], which reinvigorated the field as other proposals are also being studied and implemented [7–13]. After considerable development, especially in lattice renormalization [14–19] and perturbative matching at next-to-next-to-leading order (NNLO) [20, 21], the LaMET approach is entering the stage where the systematic errors [22] are both controllable and improvable.

In the LaMET calculation of the PDFs, lattice renormalization constitutes one of the most important systematic errors. The nonlocal quark bilinear operator $O_\Gamma(z) \equiv \bar{\psi}(z)\Gamma W(z,0)\psi(0)$ with Γ being a Dirac matrix and $z^\mu = (0, 0, 0, z)$, which defines the qPDF, suffers from a linear power divergence in the self-energy of the Wilson line $W(z,0)$ that must be completely removed before the continuum limit. So far, the most used methods are the regularization-independent momentum subtraction [14–17] and other ratio-type schemes [12, 21, 23, 24] which use the matrix element of $O_\Gamma(z)$ in an off-shell quark [14–17], a static/boosted hadron [12, 24] or the vacuum state [21, 23] as the renormalization factor. The ratio-type schemes have often been used in the coordinate space with a short-distance factorization of the matrix elements of $O_\Gamma(z)$. At large z , they introduce additional nonperturbative effects [25] that propagate to the qPDF, the Fourier transform (FT) of the matrix elements, thus contaminating the LaMET matching in x -space. To overcome this limitation, the hybrid scheme was proposed to subtract the linear divergence at large z and match the result to the $\overline{\text{MS}}$ scheme [19]. In practice, there are different ways to do the subtraction and matching [18, 19, 26], all of which have high demand for precision as the error can be amplified exponentially in z .

In this Letter we propose a procedure to subtract the linear divergence in $O_\Gamma(z)$ and match the result to the $\overline{\text{MS}}$ scheme at NNLO accuracy. We implement this method on the high-statistics lattice data for the pion valence quark PDF from Ref. [25], and achieve sub-percent precision in the subtraction. The pion valence PDF has been calculated in lattice QCD [25, 27–33] and extracted from global fits [34–37] at next-to-leading order (NLO). In this work, for the first time we apply the state-of-the-art NNLO hybrid-scheme matching to the qPDF, which shows good perturbative convergence and yields reliable determination of the pion valence PDF for

* xgao@bnl.gov

† yong.zhao@anl.gov

$0.03 \lesssim x \lesssim 0.80$ with 5–20% uncertainty.

In this study we use lattice gauges ensembles in 2+1 flavor QCD generated by HotQCD collaboration [38] using Highly Improved Staggered Quarks (HISQ) [39] with pion mass of 160 MeV in the continuum limit. We consider two lattice spacings $a = 0.04$ fm and $a = 0.06$ fm and volumes 64^4 and $48^3 \times 64$, respectively. As in our previous studies we use tadpole improved clover Wilson valence fermions on the gauge background with hypercubic (HYP) smearing [40]. The valence pion mass is set to 300 MeV. Finally, the Wilson line in $O_\Gamma(z)$ is constructed from HYP-smearred gauge links. The pion momenta $P^z = (2\pi n_z)/(L_s a)$ where $0 \leq n_z \leq 5$, with the largest momentum on the finer lattice being $P^z = 2.42$ GeV.

The qPDF $\tilde{f}_v(x, P^z, \mu)$ is defined in a boosted hadron state $|P\rangle$ with four-momentum $P^\mu = (P^t, 0, 0, P^z)$:

$$\tilde{f}_v(x, P^z, \mu) = \int \frac{d\lambda}{4\pi} e^{ix\lambda} \tilde{h}(\lambda, P^z, \mu), \quad (1)$$

where $\tilde{h}(\lambda, P^z, \mu) \equiv \langle P | O_{\gamma^t}(z) | P \rangle / P^t$, $\lambda = z P^z$, and μ is the $\overline{\text{MS}}$ renormalization scale. The operator $O_\Gamma(z)$ can be renormalized under lattice regularization as [41–43]

$$O_\Gamma^B(z) = e^{-\delta m(a)|z|} Z_O(a) O_\Gamma^R(z), \quad (2)$$

where “B” and “R” denote bare and renormalized quantities. The factor $Z_O(a)$ includes all the logarithmic ultraviolet (UV) divergences which are independent of z , while the Wilson-line mass correction $\delta m(a)$ includes the linear UV divergence and can be expressed as

$$\delta m(a) = \frac{m_{-1}(a)}{a} + m_0. \quad (3)$$

where $m_{-1}(a)$ is a series in the strong coupling $\alpha_s(1/a)$, and m_0 is an $\mathcal{O}(\Lambda_{\text{QCD}})$ constant originating from the renormalon ambiguity in $m_{-1}(a)$ [44].

The $\delta m(a)$ subtraction scheme has been used in a few calculations [18, 43, 45, 46]. This scheme becomes problematic when $z \sim a$, as the relation in Eq. (2) is plagued by lattice discretization effects, which, however, can be cancelled in ratio-type schemes. To combine the advantages of the above schemes, we adopt the hybrid scheme [19]: at short distance $0 \leq z \leq z_S$ with $a \ll z_S \ll \Lambda_{\text{QCD}}^{-1}$, we form the ratio $\tilde{h}(z, P^z, a)/\tilde{h}(z, 0, a)$ to cancel the UV divergences and discretization effects. At $z > z_S$ where the discretization effects are sufficiently suppressed, we perform a $\delta m(a)$ subtraction and determine the factor $Z_O(a)$ by imposing a continuity condition of the renormalized matrix elements at $z = z_S$.

The mass correction $\delta m(a)$ can be calculated via different methods [19]. In this work, $\delta m(a)$ is determined from the combination of static quark-antiquark potential, $V^{\text{lat}}(r)$ [38, 47] and the free energy of static quark at non-zero temperature [48, 49]. We use the following normalization scheme for $V^{\text{lat}}(r)$,

$$V^{\text{lat}}(a, r = r_0) + 2\delta m(a) = 0.95/r_0, \quad (4)$$

where $r_0 = 0.469$ fm is the Sommer scale for 2+1 flavor QCD [38], and the constant 0.95 defines the scheme. The linear divergence $m_{-1}(a)/a$ should not depend on the scheme, while m_0 does. Using this scheme combined with the recently determined values of static quark free energy with HYP smearing we determine $\delta m(a)$ for Wilson line constructed from HYP-smearred gauge links, and the results are $a\delta m(a = 0.06 \text{ fm}) = 0.1586(8)$ and $a\delta m(a = 0.04 \text{ fm}) = 0.1508(12)$.

Since m_0 in Eq. (3) is scheme dependent, a factor $e^{\bar{m}_0|z|}$ with $\bar{m}_0 \sim \mathcal{O}(\Lambda_{\text{QCD}})$ is needed to match the lattice subtraction scheme to $\overline{\text{MS}}$. It was suggested that \bar{m}_0 can be determined by equating the matched $P^z = 0$ matrix element to its $\overline{\text{MS}}$ operator product expansion (OPE) [26], where the leading-power contribution is simply given by a Wilson coefficient $C_0(\mu^2 z^2)$ known to NNLO [21, 50]. A similar method was also proposed by imposing such a condition on the vacuum expectation value of the Wilson-line in a fixed gauge [18]. In both methods, z must be small enough (0.2–0.3 fm) for perturbation theory to be reliable and the $\mathcal{O}(z^2 \Lambda_{\text{QCD}}^2)$ correction be small. But if $z \sim a$, then the discretization effects become important, so the window of z that can be used is very narrow.

Our new approach for renormalization is distinct from the existing ones by the determination of \bar{m}_0 . First we note that the leading power correction in the OPE of the $P^z = 0$ matrix element is quadratic in z , which originates from the renormalon ambiguity in $C_0(z^2 \mu^2)$ [23] or the twist-four corrections. If we add a quadratic correction term to $C_0(\mu^2 z^2)$, then we can include data points at larger z before the logarithmic $\alpha_s z^2 \ln z^2$ or subleading z^4 correction becomes important. In practice, we construct the following renormalization-group (RG) invariant ratio,

$$\lim_{a \rightarrow 0} e^{\delta m(a)(z-z_0)} \frac{\tilde{h}(z, 0, a)}{\tilde{h}(z_0, 0, a)} = e^{-\bar{m}_0(z-z_0)} \frac{C_0(z^2 \mu^2) + \Lambda z^2}{C_0(z_0^2 \mu^2) + \Lambda z_0^2}, \quad (5)$$

where $z, z_0 \gg a$ so that the discretization effects are suppressed, and the coefficient Λ is of $\mathcal{O}(\Lambda_{\text{QCD}}^2)$. According to Eq. (2), $Z_O(a)$ should cancel out in the ratio as it is independent of z , so the l.h.s. must have a well-defined continuum limit if $\delta m(a)$ includes all the linear divergences. We choose $z \geq z_0 = 0.24$ fm and find agreement between the $a = 0.04$ fm and $a = 0.06$ fm ratios at sub-percent level up to $z \sim 1.0$ fm (see App. A). Then we can fit the lattice results to the r.h.s of Eq. (5). By construction \bar{m}_0 exactly cancels the scheme-dependence of $\delta m(a)$ in Eq. (4), as changing the scheme only shifts $\delta m(a)$ by a constant, but it will inherit the $\mathcal{O}(\Lambda_{\text{QCD}})$ ambiguity in the $\overline{\text{MS}}$ scheme. Since $C_0(z^2 \mu^2)$ is only known at fixed order, we expect both \bar{m}_0 and Λ to depend on μ as well.

In principle, one can perform the above fit at finite a even without including $\delta m(a)$. However, the errors in our data are so small that the discretization effects cannot be neglected. Therefore, we first do a continuum extrapolation with a^2 -dependence [25], and then fit \bar{m}_0 , which makes the calculation of $\delta m(a)$ necessary. By

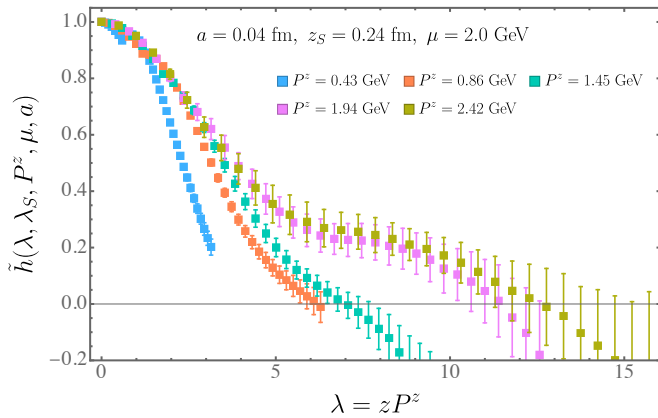


FIG. 1. Renormalized matrix elements in the hybrid scheme.

fixing $z_0 = 0.24$ fm and varying z , we obtain plateaus of both \bar{m}_0 and Λ up to $z \sim 0.4$ fm with the NNLO $C_0(z^2\mu^2)$ (see App. A). At $\mu = 2.0$ GeV, the fitted results are $\bar{m}_0 = 0.151(1)$ GeV and $\Lambda = 0.041(6)$ GeV², so the power correction cannot be neglected even at $z = 0.24$ fm. Therefore, we modify the hybrid scheme by correcting the Λz^2 term in the $P^z = 0$ matrix elements as

$$\begin{aligned} \tilde{h}(z, z_S, P^z, \mu, a) &= \frac{\tilde{h}(z, P^z, a)}{\tilde{h}(z, 0, a)} \frac{C_0(z^2\mu^2) + \Lambda z^2}{C_0(z^2\mu^2)} \theta(z_S - z) \\ &+ e^{(\delta m + \bar{m}_0)(z - z_S)} \frac{\tilde{h}(z, P^z, a)}{\tilde{h}(z_S, 0, a)} \frac{C_0(z_S^2\mu^2) + \Lambda z_S^2}{C_0(z_S^2\mu^2)} \theta(z - z_S). \end{aligned} \quad (6)$$

The continuum limit of $\tilde{h}(z, z_S, P^z, \mu, a)$ should be RG invariant, but in practice it depends on μ as C_0 is at fixed order. Such a renormalization procedure is performed through bootstrap loops so that the correlation between different P^z and z is taken care of.

The hybrid-scheme matrix elements are shown in Fig. 1. At small z , $\tilde{h}(z, P^z)$ is dominated by the leading-twist contribution. At large z , if there is no zero mode such as in the pion valence qPDF, then the spacelike correlator will exhibit an exponential decay $\propto e^{-m_{\text{eff}}|z|}$ with m_{eff} being an effective mass related to the system [51]. When plotted as a function of $\lambda = zP^z$, $\tilde{h}(\lambda, P^z)$ should scale in P^z at small λ , with slight violation due to QCD evolution. Its exponential decay will emerge at larger λ with greater P^z , while the decay constant is suppressed as m_{eff}/P^z . In the $P^z \rightarrow \infty$ limit, the exponential decay vanishes at finite λ ($z \rightarrow 0$) and only the leading-twist contribution remains, which features a power-law decay at large λ that corresponds to the Regge behavior of PDF at small x [19]. This picture is consistent with Fig. 1.

The next step is to FT the renormalized matrix elements to obtain the qPDFs. We truncate the matrix elements at z_L or $\lambda_L = z_L P^z$ before they turn negative, and extrapolate to ∞ to remove the unphysical oscillations from a truncated FT [19]. The extrapolation form we use is $Ae^{-m_{\text{eff}}|z|}/|\lambda|^d$, where A , m_{eff} and d are the parameters. The decay constant m_{eff} includes the $\mathcal{O}(\Lambda_{\text{QCD}})$ ambiguity from \bar{m}_0 , which could change its sign. Since m_{eff}

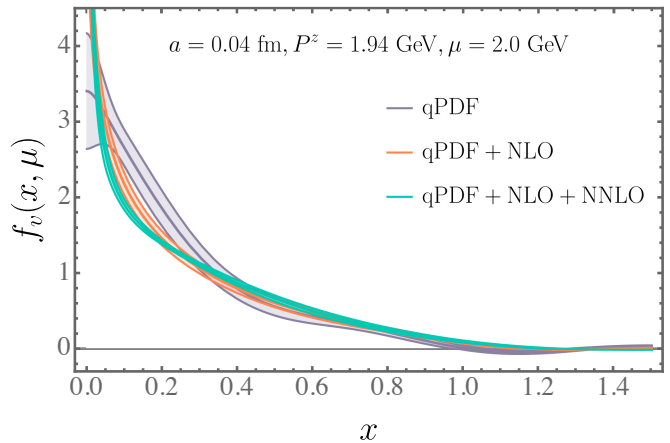


FIG. 2. Comparison of PDFs obtained from the qPDF with NLO and NNLO matching corrections.

should be independent of P^z , by fitting to the $P^z = 0$ matrix elements we find it to be positive and around 0.1 GeV, which is about the same order as the phenomenological estimate of 0.2 – 0.5 GeV in HQET [52]. Therefore, we impose the condition $m_{\text{eff}} > 0.1$ GeV as well as $A > 0$ and $d > 0$ to ensure a convergent FT on each bootstrap sample (see App. B). Since $\tilde{h}(\lambda_L)$ is close to zero and the FT converges fast with the exponential decay, the extrapolation and the condition on m_{eff} mainly affect the small- x region ($x < 1/\lambda_L$) apart from removing the unphysical oscillations. To verify this, we vary z_L (which turns out to have little impact) and the extrapolation forms, and find the qPDFs consistent with each other except for at small x ($x \lesssim 0.05$). (See App. B).

Then, we perturbatively match the qPDF $\tilde{f}_v(y, z_S, P^z)$ in the hybrid scheme to the $\overline{\text{MS}}$ PDF $f_v(x, \mu)$ through the LaMET expansion [19, 50, 53, 54]:

$$\begin{aligned} f_v(x, \mu) &= \int_{-\infty}^{\infty} \frac{dy}{|y|} C^{-1}\left(\frac{x}{y}, \frac{\mu}{yP^z}, |y|\lambda_S\right) \tilde{f}_v(y, z_S, P^z) \\ &+ \mathcal{O}\left(\frac{\Lambda_{\text{QCD}}^2}{(xP^z)^2}, \frac{\Lambda_{\text{QCD}}^2}{((1-x)P^z)^2}\right), \end{aligned} \quad (7)$$

where $\lambda_S = z_S P^z$, $z_S = 0.24$ fm, and the power corrections are controlled by the parton and spectator momenta xP^z and $(1-x)P^z$ [19]. Here C^{-1} is the inverse of the hybrid-scheme matching coefficient C which has been obtained at NNLO [55] by conversion from the $\overline{\text{MS}}$ scheme result [20, 21]. Based on Eq. (7), we can directly calculate the x -dependence of the PDF with controlled power corrections for $x_{\text{min}} \leq x \leq x_{\text{max}}$, where x_{min} and x_{max} can be determined for a target precision.

In Fig. 2 we show the results of perturbative matching, which is done for each bootstrap sample. The matching drives the qPDF to smaller x and reduces the uncertainties in the PDF at moderate x . This is because matching effectively relates the qPDF at finite P^z to the PDF in the infinite momentum frame, and the qPDF evolves to smaller x as P^z increases. The size of NNLO correction is

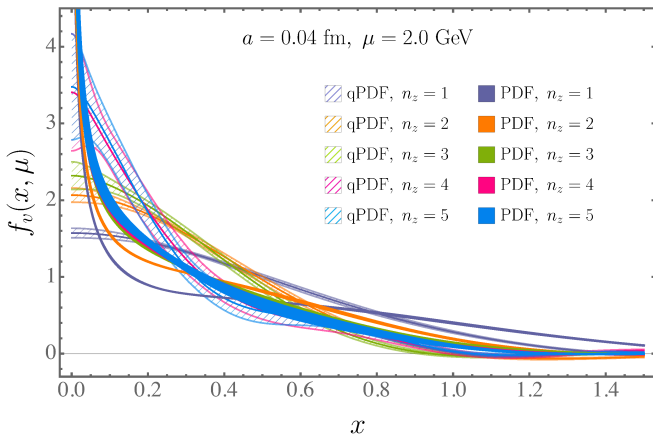


FIG. 3. The PDFs obtained from the qPDFs with NNLO matching at different $P^z = n_z \times 0.48$ GeV.

in general smaller than that of the NLO correction, which indicates good perturbative convergence, a crucial criterion for precision calculation. Besides, we also find that the uncertainty from factorization scale variation is reduced at NNLO. As $x \rightarrow 0$, the qPDF is regular because of the exponential extrapolation, while the matching correction makes it divergent, which is a sign that resummation of small- x logarithms is needed. A resummation of large logarithms is also necessary as $x \rightarrow 1$ [33]. Since the resummation effects are important only in the end-point regions, they are not considered in this analysis.

Then we compare the PDFs obtained at different P^z with NNLO matching in Fig. 3. At moderate x , the P^z -dependence is remarkably reduced, and the results appear to converge for $P^z \geq 1.45$ GeV, which strongly indicates that the perturbative matching allows for reliable predictions. According to Eq. (7), there should still be power corrections that are enhanced in both the $x \rightarrow 0$ and $x \rightarrow 1$ regions, as one can see that each PDF curve has a small nonvanishing tail at $x \geq 1$ which decreases with P^z (see also App. C 3). To estimate the size of the power corrections, we fit the PDFs obtained at $a = 0.04$ fm, $P^z = \{1.45, 1.94, 2.42\}$ GeV and $a = 0.06$ fm, $P^z = \{1.72, 2.15\}$ GeV to the *ansatz* $f_v(x) + \alpha(x)/P_z^2$ for each fixed x , where we ignore the a -dependence as the $O(a^2 P_z^2)$ effect has been shown to be less than 1% [25]. Since the least- χ^2 fit is mainly determined by the data sets at lower P^z with smaller statistical errors, which have larger power corrections, we use the result at $P^z = 2.42$ GeV instead of the fitted $f_v(x)$ as our final prediction for the PDF. The relative size of the power correction is estimated to be $\alpha(x)/[P_z^2 f_v(x)] \lesssim 0.1$ for $0.01 < x < 0.80$ and $\alpha(x)/[P_z^2 f_v(x)] \lesssim 0.05$ for $0.01 < x < 0.70$ at $P^z = 2.42$ GeV. It is surprising that the results are insensitive to P^z for x as small as 0.01, which can be explained by the fact that the qPDF contributes to the PDF at larger x under perturbative matching. However, it must be pointed out that the smallness here is only relative, as the size of $\alpha(x)/P_z^2$ still

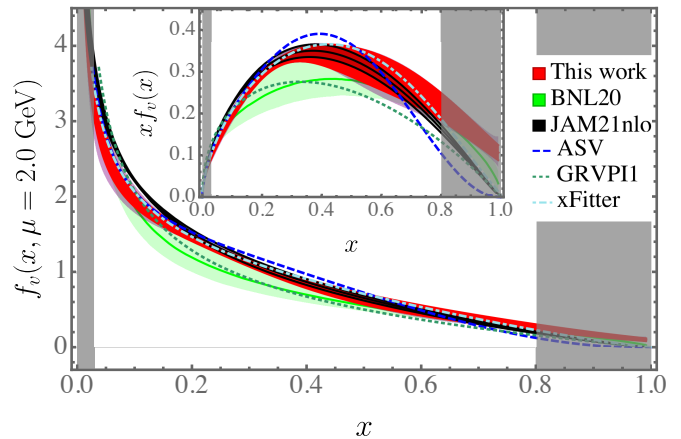


FIG. 4. Comparison of our prediction of $f_v(x)$ to global fits and BNL20. The shaded regions $x < 0.03$ and $x > 0.8$ are excluded by requiring that the estimates of $O(\alpha_s^3)$ and power corrections be smaller than 5% and 10%, respectively.

increases as $x \rightarrow 0$. To further verify this, we also calculate the PDF from the qPDF with a power-law ($A/|x|^d$) extrapolation, and find that the results are almost identical to those from the exponential extrapolation even at $x = 0.01$, so we simply use the latter to proceed.

Our final prediction for $f_v(x)$ is shown in Fig. 4. The central value is obtained from the qPDF at $a = 0.04$ fm, $z_S = 0.24$ fm, $z_L = 0.92$ fm, $\mu = 2.0$ GeV and $P^z = 2.42$ GeV with exponential extrapolation and NNLO matching. The red band represents the statistical error, and the light purple band stands for the systematic error from scale variation, which is obtained by repeating the same procedure for $\mu = 1.4$ and 2.8 GeV and evolving the matched results to $\mu = 2.0$ GeV with the NLO DGLAP equation. We demand that the relative $O(\alpha_s^3)$ matching correction at $\mu = 2.0$ GeV be smaller than 5%, which propagates to $\leq 37\%$ NLO and $\leq 14\%$ NNLO corrections and excludes the regions $x < 0.03$ and $x > 0.88$. Combining the estimates of power corrections and the statistical and scale-variation errors, we determine the PDF at $0.03 \lesssim x \lesssim 0.80$ with 5–20% uncertainty. Our result is in good agreement with the global fits by **xFitter** [35] and **JAM21nlo** [36] within the claimed region, but deviates from the **GRVP11** [34] and **ASV** [37] fits. When compared to a previous analysis of the same lattice data (**BNL20**) [25] which used the NLO OPE in coordinate space and a parameterization of the PDF, our x -space calculation shows considerably reduced uncertainties, but still agrees within errors.

In summary, we have performed a state-of-the-art lattice QCD calculation of the x -dependence of the pion valence quark PDF, where we developed a simple procedure to renormalize the qPDF in the hybrid scheme and match it to the $\overline{\text{MS}}$ PDF at NNLO accuracy. With two fine lattice spacings, we observed that the final results converge in the intermediate region of x at pion

momentum greater than 1.45 GeV, which allowed us to reliably estimate the systematic errors. The precision of this calculation can be improved with higher statistics for simulating the matrix elements at long distance and larger boost momentum.

Our renormalization procedure can also be incorporated into lattice calculations of other parton physics such as the gluon PDFs, distribution amplitudes, generalized parton distributions and transverse momentum distributions. With the systematics being under control, we can expect lattice QCD to provide reliable predictions for these quantities in the future.

ACKNOWLEDGMENTS

We thank Vladimir Braun, Xiangdong Ji, Nikhil Karthik, Yizhuang Liu, Antonio Pineda, Yushan Su and Jianhui Zhang for valuable communications. This material is based upon work supported by: (i) The U.S. Department of Energy, Office of Science, Office of Nuclear Physics through Contract No. DE-SC0012704 and No. DE-AC02-06CH11357; (ii) The U.S. Department of Energy, Office of Science, Office of Nuclear Physics and Office of Advanced Scientific Computing Research within the framework of Scientific Discovery through Advance Computing (SciDAC) award Computing the Properties of Matter with Leadership Computing Resources; (iii) The U.S. Department of Energy, Office of Science, Office of Nuclear Physics, within the framework of the TMD Topical Collaboration. (iv) XG is partially supported by the NSFC under the grant number 11775096 and the Guangdong Major Project of Basic and Applied Basic Research No. 2020B0301030008. (v) SS is supported by the National Science Foundation under CAREER Award PHY-1847893 and by the RHIC Physics Fellow Program of the RIKEN BNL Research Center.. (vi) This research used awards of computer time provided by the INCITE and ALCC programs at Oak Ridge Leadership Computing Facility, a DOE Office of Science User Facility operated under Contract No. DE-AC05-00OR22725. (vii) Computations for this work were carried out in part on facilities of the USQCD Collaboration, which are funded by the Office of Science of the U.S. Department of Energy. (viii) YZ is partially supported by an LDRD initiative at Argonne National Laboratory under Project No. 2020-0020.

Appendix A: Hybrid scheme renormalization

1. Definition of scheme

As has been described in the main text, the hybrid scheme renormalization includes two parts:

- For $z \leq z_S$, we form the ratio of bare matrix ele-

ments [12],

$$\frac{\tilde{h}(z, P^z, a)}{\tilde{h}(z, 0, a)}, \quad (\text{A1})$$

which has a well-defined continuum limit and is renormalization group (RG) invariant.

- For $z \geq z_S$, the renormalization is done through the relation

$$\tilde{h}(z, P^z, a) = e^{-\delta m(a)|z|} Z_O(a) \tilde{h}_R(z, P^z). \quad (\text{A2})$$

To determine $\delta m(a)$ we use the additive renormalization constant, $c_Q(a) = \delta m(a)$, which is obtained in Ref. [49] from the analysis of the free energy of a static quark, $F_Q(T)$, at non-zero temperature T with the normalization condition in Eq. (4). Recently F_Q has been calculated using one step of HYP smearing [56], and it was found that HYP smearing does not affect the temperature dependence of $F_Q(T)$, but only shifts it by an additive constant. Therefore, we have $F_Q^{B,1}(T) + \delta m(a) = F_Q^{B,0}(T) + c_Q(a)$ with superscripts 0 and 1 referring to the number of HYP smearing steps in the bare free energy of the static quark. Using the lattice results for $F_Q^{B,0}(T)$ and $F_Q^{B,1}(T)$ obtained on $N_\tau = 12$ lattices and temperatures corresponding to $a = 0.04$ fm and $a = 0.06$ fm (where cutoff effects can be neglected), as well as the values of c_Q from Table X of Ref. [49] for $\beta = 7.825$ ($a = 0.04$ fm) and $\beta = 7.373$ ($a = 0.06$ fm), we obtain $\delta m(a)$. The results are $a\delta m(a = 0.06 \text{ fm}) = 0.1586(8)$ and $a\delta m(a = 0.04 \text{ fm}) = 0.1508(12)$. The renormalization factor $Z_O(a)$ is determined by requiring that $\tilde{h}_R(z, P^z)$ be equal to the ratio in Eq. (A1) at $z = z_S$, which leads to

$$Z_O(a) = e^{\delta m(a)|z_S|} \tilde{h}(z_S, 0, a). \quad (\text{A3})$$

First of all, to test how well the subtraction of $\delta m(a)$ can remove the linear divergences in $\tilde{h}(z, P^z, a)$, we construct the ratio in Eq. (5),

$$\tilde{R}(z, z_0, a) \equiv e^{\delta m(a)(z-z_0)} \frac{\tilde{h}(z, 0, a)}{\tilde{h}(z_0, 0, a)}, \quad (\text{A4})$$

where $z_0 = 0.24$ fm for both lattice spacings. According to Eq. (2), the renormalization factor $Z_O(a)$ cancels out in the ratio, so if $\delta m(a)$ includes all the linear divergences, then $\tilde{R}(z, z_0, a)$ should have a well-defined continuum limit.

Our lattice results for the above ratio with $z_0 = 0.24$ fm is shown in Fig. 5. As one can see, the differences between the ratios at $a = 0.04$ fm and 0.06 fm are at sub-percent level, which clearly shows that the linear divergences have been sufficiently subtracted by $\delta m(a)$.

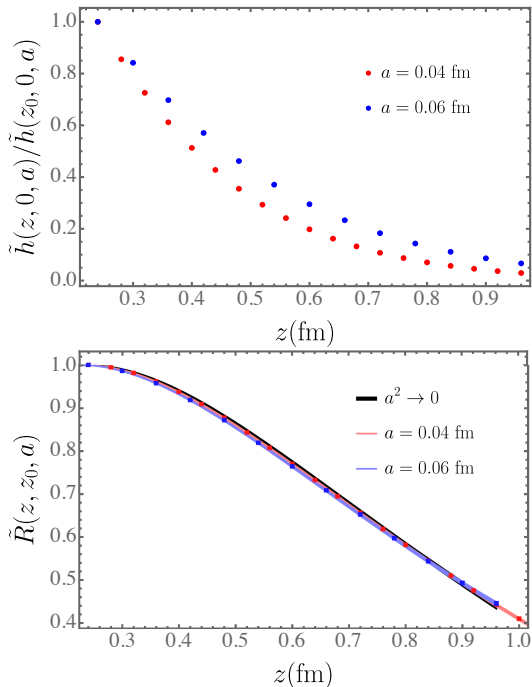


FIG. 5. Upper panel: ratios of bare lattice matrix elements without the Wilson-line mass subtraction. Lower panel: the ratio in Eq. (A4) with Wilson-line mass subtraction. The red and blue points are for $a = 0.04$ fm and 0.06 fm. The red and blue bands are interpolations of the points, and the gray band is the continuum extrapolation of them with a^2 -dependence.

In the continuum limit,

$$\lim_{a \rightarrow 0} \tilde{R}(z, z_0, a) = \tilde{R}(z, z_0), \quad (\text{A5})$$

which is related to the $\overline{\text{MS}}$ scheme through

$$\tilde{R}(z, z_0) = e^{-\Delta m_0 |z|} \tilde{R}^{\overline{\text{MS}}}(z, z_0), \quad (\text{A6})$$

where Δm_0 is finite and cancels the subtraction-scheme-dependence in $\tilde{R}(z, z_0)$. The $\overline{\text{MS}}$ scheme ratio

$$\tilde{R}^{\overline{\text{MS}}}(z, z_0) = \frac{\tilde{h}^{\overline{\text{MS}}}(z, 0, \mu)}{\tilde{h}^{\overline{\text{MS}}}(z_0, 0, \mu)} \quad (\text{A7})$$

is also RG invariant, although the matrix elements in the ratio depend on the $\overline{\text{MS}}$ scale μ respectively.

When $z, z_0 \ll \Lambda_{\text{QCD}}^{-1}$, the $\overline{\text{MS}}$ matrix element can have an operator product expansion (OPE) that goes as

$$\tilde{h}^{\overline{\text{MS}}}(z, 0, \mu) = e^{-m_0^{\overline{\text{MS}}}|z|} [C_0(z^2\mu^2) + z^2 C_2(z^2\mu^2) \langle P | O_{\text{tw}4}(\mu) | P \rangle + \dots], \quad (\text{A8})$$

where $m_0^{\overline{\text{MS}}}$ is the $\mathcal{O}(\Lambda_{\text{QCD}})$ renormalon ambiguity from the Wilson line self-energy renormalization [23], $O_{\text{tw}4}(\mu)$ is a twist-four operator (for example, $\bar{\psi} D^2 \psi$ or $g\bar{\psi} \sigma_{\mu\nu} F^{\mu\nu} \psi$), C_0 and C_2 are perturbative coefficient functions, and “...” denotes contributions at

higher twists. The leading-twist contribution is proportional to $\langle P | \bar{\psi} \gamma^t \psi | P \rangle / (2P^t)$ which is trivially one due to vector current conservation. Since $\tilde{h}^{\overline{\text{MS}}}(z, 0, \mu)$ is multiplicatively renormalizable, both $C_0(z^2\mu^2)$ and $C_2(z^2\mu^2) \langle P | O_{\text{tw}4}(\mu) | P \rangle$ must satisfy RG equations with the same anomalous dimension, which is known to next-to-next-to-leading (N³LO) order [57].

Note that $m_0^{\overline{\text{MS}}}$ is analogous to the mass renormalization in heavy-quark effective theory (HQET) [52], which is of UV origin and cannot be attributed to any short-distance condensate. Instead, it appears as a residual mass term in the HQET Lagrangian and exists in $\tilde{h}^{\overline{\text{MS}}}(z, 0, \mu)$ at all z , i.e.,

$$\tilde{h}^{\overline{\text{MS}}}(z, 0, \mu) = e^{-m_0^{\overline{\text{MS}}}|z|} \tilde{h}_0^{\overline{\text{MS}}}(z, 0, \mu), \quad (\text{A9})$$

where $\tilde{h}_0^{\overline{\text{MS}}}(z, 0, \mu)$ at short distance reduces to the OPE series in the brackets of Eq. (A8).

Due to the ambiguity in summing the perturbative series in $C_0(z^2\mu^2)$, there are $\mathcal{O}(\Lambda_{\text{QCD}}^{2n})$ IR renormalons in the leading-twist contribution that should be cancelled by those from higher-twist condensates, along with the $\mathcal{O}(\Lambda_{\text{QCD}})$ UV renormalon to be cancelled by $m_0^{\overline{\text{MS}}}$ [23, 52]. Both the UV and IR renormalon contributions cannot be well defined unless one specifies how to sum the perturbative series in $C_0(z^2\mu^2)$ to all orders, which, however, is unknown as $C_0(z^2\mu^2)$ has been calculated to only NNLO so far [21].

The renormalons have been studied extensively for the Polyakov loop and plaquette in lattice QCD [44, 58–61]. In lattice perturbation theory, one has to compute the perturbative series to very high orders of α_s in order to see the renormalon effects. Nevertheless, in the $\overline{\text{MS}}$ scheme, the OPE with Wilson coefficient at a few loop orders and the condensate term, turns out to be successful in describing the static potential at short distance up to ~ 0.25 fm [62]. One explanation is that α_s in the $\overline{\text{MS}}$ scheme is larger than that in lattice perturbation theory, so the renormalon effect which is of $\mathcal{O}(\alpha_s^n)$ with $n \sim (2\pi)/(\beta_0\alpha_s)$ becomes significant at lower loop orders. This situation is also similar to the OPE in QCD sum rules [63–67], which works well in phenomenological applications. The reason behind such success is probably due to a proper choice of the renormalization scale μ so that $\alpha_s(\mu)$ is small enough for the perturbative series to converge, while the μ -dependent effects in the condensate remain insignificant as they should be of the same magnitude of highest order in the truncated perturbative series [66, 67]. Therefore, we approximate Eq. (A8) as

$$\tilde{h}_{\text{FO}}^{\overline{\text{MS}}}(z, 0, \mu) \approx e^{-m_0^{\overline{\text{MS}}}(\mu)|z|} [C_0^{\text{FO}}(z^2\mu^2) + \Lambda(\mu)z^2], \quad (\text{A10})$$

where “FO” stands for fixed order, $\Lambda(\mu)$ is a parameter of $\mathcal{O}(\Lambda_{\text{QCD}}^2)$, and we ignore the higher power corrections. The μ dependence of the parameters $m_0^{\overline{\text{MS}}}$ and Λ is understandable because this approximation is valid for a small

window of μ , and they also depend on the perturbative orders in C_0^{FO} if the latter does not converge fast. Note that the although the model in Eq. (A10) is not guaranteed to satisfy the RG equation for $\tilde{h}^{\overline{\text{MS}}}(z, 0, \mu)$, we argue that within the range of μ where it can describe the physical results, the μ -dependence in the power correction term, which is already suppressed, is weak and can be ignored.

Based on the above approximation, we can fit our lattice results of the ratio in Eq. (A4) to the following *ansatz*,

$$\tilde{R}(z, z_0) = e^{-\bar{m}_0(\mu)(z-z_0)} \frac{C_0^{\text{FO}}(z^2\mu^2) + \Lambda(\mu)z^2}{C_0^{\text{FO}}(z_0^2\mu^2) + \Lambda(\mu)z_0^2}, \quad (\text{A11})$$

where

$$\bar{m}_0(\mu) = \Delta m_0 + m_0^{\overline{\text{MS}}}(\mu). \quad (\text{A12})$$

Since the factorization of qPDF in the x -space has only been derived perturbatively [5, 54] without the ambiguity term $e^{-m_0^{\overline{\text{MS}}}(\mu)|z|}$, it is natural to match $\tilde{R}(z, z_S)$ at $z \geq z_S$ to the ratio of $\tilde{h}_0^{\overline{\text{MS}}}$ as

$$e^{\bar{m}_0(\mu)(z-z_S)} \tilde{R}(z, z_S) = \frac{\tilde{h}_0^{\overline{\text{MS}}}(z, P^z, \mu)}{\tilde{h}_0^{\overline{\text{MS}}}(z_S, 0, \mu)}. \quad (\text{A13})$$

Moreover, since $\Lambda(\mu)$ will also be fitted from the lattice results, we can correct the higher-twist contribution in $\tilde{h}_0^{\overline{\text{MS}}}(z_S, 0, \mu)$ through the multiplication

$$\frac{\tilde{h}_0^{\overline{\text{MS}}}(z, P^z, \mu) C_0^{\text{FO}}(z_S^2\mu^2) + \Lambda(\mu)z_S^2}{\tilde{h}_0^{\overline{\text{MS}}}(z_S, 0, \mu) C_0^{\text{FO}}(z_S^2\mu^2)}, \quad (\text{A14})$$

which corresponds to the treatment in Eq. (6). Eventually, the continuum matrix element we obtain is

$$\begin{aligned} \tilde{h}(z, z_S, P^z) &= \frac{\tilde{h}_0^{\overline{\text{MS}}}(z, P^z, \mu)}{C_0^{\text{FO}}(z^2\mu^2)} \theta(z_S - |z|) \\ &+ \frac{\tilde{h}_0^{\overline{\text{MS}}}(z, P^z, \mu)}{C_0^{\text{FO}}(z_S^2\mu^2)} \theta(|z| - z_S), \end{aligned} \quad (\text{A15})$$

which is different from the $\overline{\text{MS}}$ scheme through a perturbative matching that does not include large $\ln(z^2\mu^2)$ for all z as long as $z_S \ll \Lambda_{\text{QCD}}^{-1}$. Therefore, the qPDF defined as Fourier transform of $\tilde{h}(z, z_S, P^z)$ is still factorizable. In principle $\tilde{h}(z, z_S, P^z)$ should be RG invariant if C_0^{FO} is obtained at all orders, while at finite orders the result can still depend on μ as \bar{m}_0 and Λ do.

By default $\bar{m}_0(\mu)$ cancels the subtraction-scheme dependence of $\delta m(a)$. However, since there is always $\mathcal{O}(\Lambda_{\text{QCD}})$ ambiguity in $m_0^{\overline{\text{MS}}}(\mu)$ due to the arbitrariness in summing the perturbative series in $C_0(\mu^2 z^2)$, $\bar{m}_0(\mu)$ still suffers from such uncertainty. Nevertheless, we argue that $C_0^{\text{FO}}(\mu^2 z^2)$ at NNLO is different from a particular summation prescription by $\mathcal{O}(\alpha_s^3)$ contributions, which

cannot be smaller than the ambiguity in $m_0^{\overline{\text{MS}}}(\mu)$ as the latter reflects the uncertainty in summing divergent perturbative series at sufficiently high orders. Therefore, we can attribute the renormalon ambiguity in $\bar{m}_0(\mu)$ to higher loop-order effects and estimate the latter by varying μ . Notably, unlike the usual estimate of perturbation theory uncertainty in collider phenomenology, we should not simply vary μ by a factor of 2 or 1/2. Instead, we should carefully choose the range of μ such that higher-order perturbative corrections are small. If μ is too small, then $\alpha_s(\mu)$ becomes too large; if μ is too large, then we need to resum the large $\ln(z^2\mu^2)$ in $C_0(z^2\mu^2)$, which inevitably requires evolving α_s to $\mu^2 = 1/z^2$ which is not far from the IR region.

In our analysis, we scan μ within [0.9, 2.0] GeV for C_0^{NLO} and [1.4, 3.2] GeV for C_0^{NNLO} to study the scale dependence.

2. Fitting of \bar{m}_0 and $\Lambda(\mu)$

Currently, the Wilson coefficient $C_0(\mu^2 z^2)$ is known to NNLO [21] and its anomalous dimension has been calculated at N³LO [57],

$$\begin{aligned} C_0(\mu^2 z^2, \alpha_s(\mu)) &= a_s \left(2L + \frac{10}{3} \right) \\ &+ a_s^2 \left[\frac{13}{2} L^2 + \frac{1461 + 28\pi^2}{54} L + \frac{38127 - 824\pi^2 - 4032\zeta(3)}{648} \right] \\ &+ a_s^3 \left[\frac{143}{6} L^3 + \left(\frac{6127}{36} + \frac{91\pi^2}{27} \right) L^2 \right. \\ &\quad \left. + \frac{690939 + 760\pi^4 - 8976\pi^2 - 94068\zeta(3)}{972} L + 400 \right] \\ &+ \mathcal{O}(a_s^4), \end{aligned} \quad (\text{A16})$$

where $a_s = \alpha_s(\mu)/(2\pi)$, $\mathbf{z}^2 = z^2 e^{2\gamma_E}/4$, $L = \ln(\mu^2 \mathbf{z}^2)$, and the constant 400 is an estimate of the constant part of the $\mathcal{O}(a_s^3)$ correction by assuming that it grows as a geometric series in the order of a_s .

We also consider the RG improved (RGI) Wilson coefficient [33]

$$\begin{aligned} C_0^{\text{RGI}}(\mu^2, \mathbf{z}^2) &= C_0(1, \alpha_s(\mathbf{z}^{-1})) \\ &\times \exp \left[\int_{\mathbf{z}^{-1}}^{\mu} d\alpha_s(\mu') \frac{\gamma_{\mathcal{O}}(\alpha(\mu'))}{\beta(\alpha_s(\mu'))} \right], \end{aligned} \quad (\text{A17})$$

where $\gamma_{\mathcal{O}}$ is the anomalous dimension of the operator $\mathcal{O}_{\Gamma}(z, \mu)$, and $\beta(\alpha_s(\mu)) = d\alpha_s(\mu)/d\ln\mu^2$. In this way, we can first factor out the evolution factor in Eq. (A10) as it must be satisfied by the full matrix element $\tilde{h}^{\overline{\text{MS}}}(z, 0, \mu)$, and therefore construct the ratio $\tilde{R}(z, z_0)$ in an explicitly μ -independent way.

We compare C_0 and C_0^{RGI} at NLO, NNLO and N³LO at $\mu = 2.0$ GeV in Fig. 6. The strong coupling constants at each perturbative order are defined by the corresponding $\Lambda_{\text{QCD}}^{\overline{\text{MS}}}$ with one-, two- and three- loop β

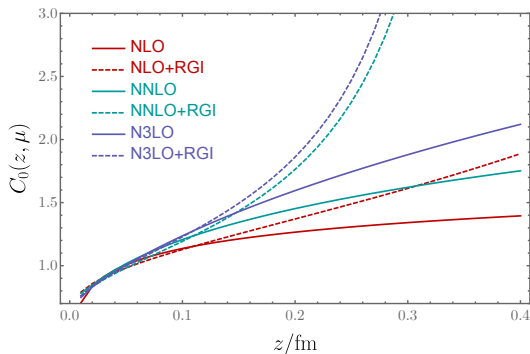


FIG. 6. The fixed-order and RGI Wilson coefficients $C_0(z^2\mu^2)$ up to N³LO.

functions and $n_f = 3$, which are fixed by matching to $\alpha_s(\mu = 2 \text{ GeV}) = 0.293$. The latter is obtained from $\Lambda_{\text{QCD}}^{\overline{\text{MS}}} = 332 \text{ MeV}$ with five-loop β -function and $n_f = 3$, as has been calculated using the same lattice ensembles [68]. As one can see, at $z > 0.2 \text{ fm}$ the RGI Wilson coefficients start to deviate significantly from the fixed-order ones, which is mainly due to the large value of α_s as in RGI Wilson coefficients as we evolve from μ to $1/z$. This indicates that at $z > 0.2 \text{ fm}$, the scale uncertainty in the perturbative series is significant due to the enhancement of non-perturbative effects, and to use OPE we should work at very short distances ($z < 0.2 \text{ fm}$). However, there will not be enough room for varying z to satisfy $z \gg a$ so that discretization effects are suppressed. Therefore, in our analysis we loosen our requirement for very small z by only using the *ansatz* in Eq. (A11) and not considering the RGI Wilson coefficients.

In Fig. 7a, we plot an effective mass $\bar{m}_0^{\text{eff}}(z)$ which is defined as

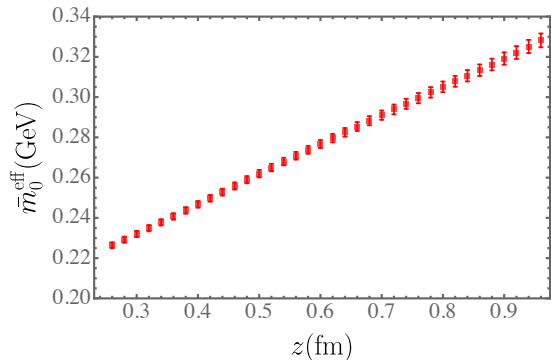
$$\bar{m}_0^{\text{eff}}(z)(z - z_0) \equiv -\ln \frac{\tilde{h}(z, 0, a)}{\tilde{h}(z_0, 0, a)} + \ln \frac{C_0^{\text{NNLO}}(z^2\mu^2)}{C_0^{\text{NNLO}}(z_0^2\mu^2)}, \quad (\text{A18})$$

where $\mu = 2.0 \text{ GeV}$. If the twist-four condensate is negligible, then we should expect a plateau in z , but Fig. 7a shows that it has an almost constant nonzero slope at z from 0.24 fm up to 1.0 fm . In Fig. 7b we plot its slope

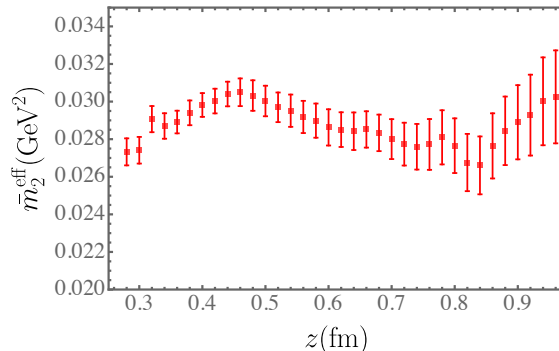
$$\bar{m}_2^{\text{eff}}(z) = \frac{\bar{m}_0^{\text{eff}}(z) - \bar{m}_0^{\text{eff}}(z - a)}{a}, \quad (\text{A19})$$

which is consistent with being constant for a wide range of z . This suggests that there is considerable quadratic z -dependence from the twist-four condensate, as included in the *ansatz* in Eq. (A11).

Our results for \bar{m}_0 and Λ fitted from $\tilde{R}(z, z_0)$ for $z_0 < z < z_{\text{max}}$ with $z_0 = 0.24 \text{ fm}$ are shown in Fig. 8. As one can see, the two parameters remain constant in z_{max} up to around 0.5 fm within a small window of μ , which is different with the NLO and NNLO Wilson coefficients. At larger z , the higher-twist and $\alpha_s \ln(z^2\mu^2)$ effects become significant, which can no longer be described by the



(a)



(b)

FIG. 7. Effective mass $\bar{m}_0^{\text{eff}}(z)$ (a) and its slope $\bar{m}_2^{\text{eff}}(z)$ (b) vs z .

simple *ansatz* in Eq. (A11). In this work, we use $\tilde{R}(z, z_0)$ at $0.24 \text{ fm} < z < 0.4 \text{ fm}$ to fit the parameters at all μ as input for the hybrid scheme renormalization and matching. To estimate the uncertainty from the choice of μ , we will match the qPDFs obtained at different μ to the corresponding PDFs, and then evolve the final results to $\mu = 2.0 \text{ GeV}$ for comparison.

Appendix B: Fourier transform (FT)

The qPDF is defined as the FT of $\tilde{h}(z, z_S, P^z)$ or $\tilde{h}(\lambda, \lambda_S, P^z)$,

$$\tilde{f}(x, z_S, P^z) = \int \frac{d\lambda}{2\pi} e^{ix\lambda} \tilde{h}(\lambda, \lambda_S, P^z). \quad (\text{B1})$$

Since $\tilde{h}(\lambda, \lambda_S, P^z)$ is perturbatively matched from the $\overline{\text{MS}}$ scheme, the factorization formula should still be valid for the corresponding qPDF $\tilde{f}(x, z_S, P^z)$ [19]. Therefore, we should integrate over all z in the FT to obtain the x -dependence of the qPDF. However, due to finite lattice size effects, worsening signal-to-noise ratio and other systematics at large z , we have to truncate $\tilde{h}(z, z_S, P^z)$ at $z = z_L$ and extrapolate to $z \rightarrow \infty$ to complete the FT. As a result, the small- x ($x \lesssim 1/\lambda_L$) region is the most sensitive to the extrapolation model, and the corresponding systematic uncertainty cannot be well controlled. On the

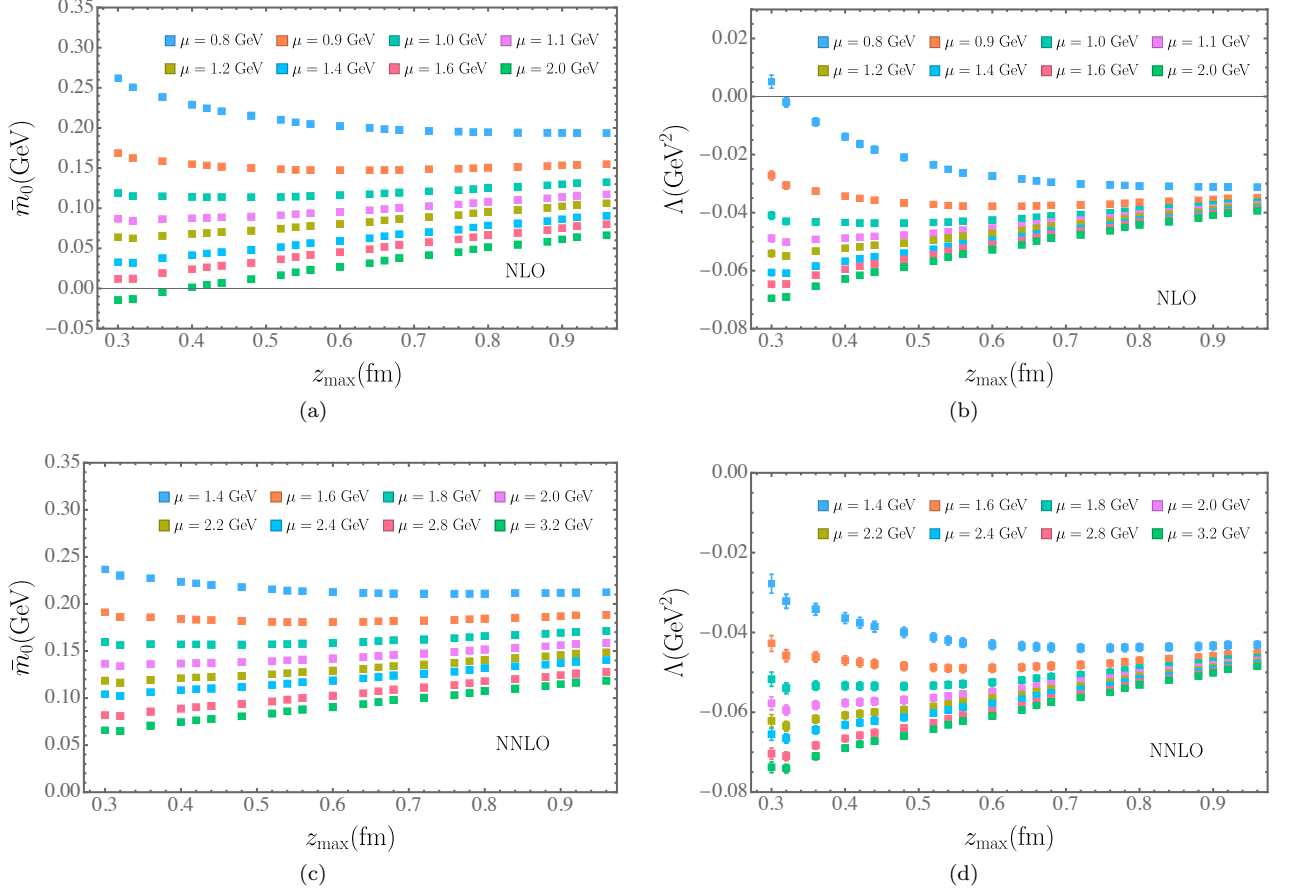


FIG. 8. Results for $\bar{m}_0(\mu)$ (a) and $\Lambda(\mu)$ (b) fitted from $\tilde{R}(z, z_0)$ for $z_0 < z < z_{\max}$ and $z_0 = 0.24$ fm, with NLO and NNLO Wilson coefficients at various values of μ .

other hand, the reliability of the $x \gtrsim 1/\lambda_L$ region depends on the premises that the $\tilde{h}(z)$ is small at $z = z_L$ and exhibits an exponential decay when z_L is large enough. The first condition is easy to understand as a truncated FT will lead to an unphysical oscillation in the x -space with amplitude proportional to $|\tilde{h}(z_L)|$, while the exponential decay guarantees that the FT converges fast and the qPDF at $x \gtrsim 1/\lambda_L$ has very little dependence on the specific model used in the extrapolation.

In this section, we first derive that the equal-time correlator in a hadron state does exhibit an exponential decay at large distances, then we demonstrate that including this constraint in the extrapolation will lead to a reliable FT in the moderate-to-large x region. Finally, we perform the extrapolated FT on our lattice results.

1. Matrix elements at large z

To begin with, let us consider a current-current correlation in the vacuum, $\langle \Omega | J_5(x) J_5(0) | \Omega \rangle$, where $J_5 = \bar{q} \gamma_5 q$ and $x^2 < 0$. If we ignore the existence of zero modes and

only consider gapped vacuum excitations, then

$$\begin{aligned}
 & \langle \Omega | J_5(x) J_5(0) | \Omega \rangle \\
 &= \sum_n \int \frac{d^3 k_n}{(2\pi)^3 2E_{k_n}} \langle \Omega | J_5(x) | n \rangle \langle n | J_5(0) | \Omega \rangle \\
 &= \sum_n \int \frac{d^3 k_n}{(2\pi)^3 2E_k} \langle \Omega | J_5(0) | n \rangle \langle n | J_5(0) | \Omega \rangle e^{-ix \cdot k_n} \\
 &= \sum_n |Z_n|^2 \int \frac{d^4 k_n}{(2\pi)^4} \frac{e^{-ix \cdot k_n}}{k_n^2 - m_n^2 + i0} \\
 &= -\frac{i}{4\pi^2} \sum_n |Z_n|^2 \frac{m_n}{\sqrt{-x^2}} K_1(m_n \sqrt{-x^2}). \quad (\text{B2})
 \end{aligned}$$

where Z_n is the overlap between the operator $J_5(x)$ and intermediate state $|n\rangle$. Here m_n is the mass of the intermediate state particle, and K_n is the modified Bessel function of the second kind. Then, since

$$\lim_{|x| \rightarrow \infty} \frac{m_n}{\sqrt{-x^2}} K_1(m_n \sqrt{-x^2}) = \sqrt{\frac{\pi}{2}} \frac{\sqrt{m_n}}{|x|^{\frac{3}{2}}} e^{-m_n |x|}, \quad (\text{B3})$$

The correlation function should, therefore, be dominated by the exponential decay of the lowest-lying state that overlaps with $J_5(x)$.

When the external state is a static hadron, it has also been shown that the spacelike correlations exhibit an exponential decay at large distance [51].

We are interested in equal-time quark bilinear correlators in a boosted hadron state, which can be expressed in terms of the product of two ‘‘heavy-light’’ currents [41, 43], where the ‘‘heavy quark’’ $h_{\hat{x}}$ is an auxiliary field defined along the \hat{x} direction, similar to that in HQET.

Let us choose the external state to be a pion. According to Lorentz covariance, we can decompose the correlation as

$$\begin{aligned} & \langle \pi(p) | \bar{q}(x) \gamma^\mu h_{\hat{x}}(x) \bar{h}_{\hat{x}}(0) q(0) | \pi(p) \rangle \\ & = p^\mu f_p(p \cdot x, x^2) + x^\mu f_x(p \cdot x, x^2), \end{aligned} \quad (\text{B4})$$

where the scalar functions $f_{p,x}(p \cdot x, x^2)$ are analytic functions of $p \cdot x$ and x^2 . We can select the index μ such that $x^\mu = 0$. For example, we can choose $\mu = z$ when $x^\mu = (t, 0, 0, 0)$ or $\mu = t$ when $x^\mu = (0, 0, 0, z)$. The HQET corresponds to the timelike case, as

$$\begin{aligned} p^z f_p(p \cdot x, x^2) & = \sum_n \int \frac{d^3 k_n}{(2\pi)^3 2E_{k_n}} e^{-ix \cdot (k_n - m_Q v - p)} \\ & \times \langle \pi(p) | \bar{q} \Gamma h_v | n \rangle \langle n | \bar{h}_v q | \pi(p) \rangle, \end{aligned} \quad (\text{B5})$$

where h_v is the effective heavy-quark field moving with velocity v^μ and related to the QCD heavy quark Q by the projection

$$h_v(x) = e^{im_Q v \cdot x} \frac{1 + \not{v}}{2} Q(x). \quad (\text{B6})$$

The lowest intermediate state $|H(v)\rangle$ is a heavy-light meson with mass $m_H = m_Q + \bar{\Lambda}$ and momentum $k^\mu = m_H v^\mu$, where m_Q is the heavy quark pole mass, and $\bar{\Lambda}$ can be interpreted as the mass of the constituent light quark or binding energy. Both $\bar{\Lambda}$ and m_Q have $\mathcal{O}(\Lambda_{\text{QCD}})$ renormalon ambiguities which cancel between each other. In the $\Lambda_{\text{QCD}}/m_Q \rightarrow 0$ limit, $\bar{\Lambda}$ should be independent of the heavy quark mass, but can depend on the light quark mass.

The matrix element $\langle \pi(p) | \bar{q} \Gamma h_v | H(v) \rangle$ is given by the transition form factors [69],

$$\begin{aligned} & \langle \pi(p) | \bar{q} \Gamma h_v | H(v) \rangle \\ & = -\text{Tr} \left\{ \gamma_5 \left[f_1(v \cdot p) + f_2(v \cdot p) \frac{\not{p}}{v \cdot p} \right] \Gamma \mathcal{M}(v) \right\}, \end{aligned} \quad (\text{B7})$$

where the form factors f_1 and f_2 only depend on $v \cdot p$ in HQET, and the projection operator $\mathcal{M}(v)$ depends on the spin of the heavy-light meson $H(v)$,

$$\mathcal{M}(v) = \frac{1 + \not{v}}{2} \begin{cases} -\gamma_5, & \text{for } J^P = 0^-, \\ \not{\epsilon}, & \text{for } J^P = 1^-, \end{cases} \quad (\text{B8})$$

with ϵ^μ being the polarization vector for vector mesons. Therefore,

$$\langle \pi(p) | \bar{q} \gamma^\mu h_v | H(v) \rangle = 2f_1(v \cdot p) v^\mu + 2f_2(v \cdot p) p^\mu, \quad (\text{B9})$$

$$\langle \pi(p) | \bar{q} h_v | H(v) \rangle = 2f_1(v \cdot p) + 2f_2(v \cdot p). \quad (\text{B10})$$

Then, the correlation function becomes

$$\begin{aligned} p^z f_p(p \cdot x, x^2) & \approx 4m_Q^2 \sum_n \int \frac{d^3 \vec{v}}{(2\pi)^3 2\sqrt{1 + \vec{v}^2}} \\ & \times e^{-i(\bar{\Lambda}\sqrt{1 + \vec{v}^2} - p^0)x^0} (f_1 + f_2)(f_1 v^z + f_2 p^z). \end{aligned} \quad (\text{B11})$$

Note that when $x^0 \rightarrow \infty$, $x^0 \bar{\Lambda} \sqrt{1 + \vec{v}^2} \geq x^0 \bar{\Lambda}$ constitutes a large phase, so the integrand is quickly oscillating and should be suppressed. To have a naive estimate, let us assume f_1 and f_2 are constant in $v \cdot p$, and the remaining integral is simply

$$\begin{aligned} & \int \frac{d^3 \vec{v}}{(2\pi)^3 2\sqrt{1 + \vec{v}^2}} e^{-i(\bar{\Lambda}\sqrt{1 + \vec{v}^2} - p^0)x^0} \\ & = \frac{1}{4\pi^2} K_1 \left(\bar{\Lambda} \sqrt{-x_0^2} \right) \frac{e^{ip^0 x_0}}{\bar{\Lambda} \sqrt{-x_0^2}} \\ & = \frac{1}{4\pi^2} K_1 \left(\bar{\Lambda} \sqrt{-x^2} \right) \frac{e^{ip \cdot x}}{\bar{\Lambda} \sqrt{-x^2}}, \end{aligned} \quad (\text{B12})$$

where we first obtained the result for imaginary x^0 and then analytically continued back to the real axis.

Then, using Lorentz invariance and analyticity, we can obtain the result for $x^2 < 0$, which corresponds to the equal-time correlator that we calculate in this work. At large separation, we have

$$\lim_{|x| \rightarrow \infty} f_p(p \cdot x, x^2) \propto m_Q^2 \frac{e^{-\bar{\Lambda}|x|}}{(\bar{\Lambda}|x|)^{\frac{3}{2}}} e^{ip \cdot x}, \quad (\text{B13})$$

which also exhibits an exponential behavior with decay constant $\bar{\Lambda}$. Moreover, the correlation also includes a phase $e^{ip \cdot x}$ which becomes $\cos(p \cdot x)$ in the case of the valence quark distribution. Another important takeaway is that $\bar{\Lambda}$ is a Lorentz-invariant quantity and should be independent of the external momentum.

However, it must be pointed out that the conclusion in Eq. (B13) is based on a rather crude approximation that f_1 and f_2 are constant in $v \cdot p$. In practice, the transition form factors could have a pole at the mass of a heavy-light meson created by the current $\bar{q} \gamma^\mu h_v$ or $\bar{h}_v q$, which is different from m_H for the intermediate state $|H(v)\rangle$. As a result, the binding energy $\bar{\Lambda}$ would also be different. If we take this into account in Eq. (B11), then the result will exhibit a more complicated asymptotic behavior at large distance,

$$\lim_{|x| \rightarrow \infty} f_p(p \cdot x, x^2) \propto \frac{e^{-\bar{\Lambda}|x|}}{|x|^d} g[p \cdot x, \cos(p \cdot x), \sin(p \cdot x)], \quad (\text{B14})$$

where the decay constant $\bar{\Lambda}$ should vary among the different binding energies for the heavy-light mesons, which is similar to the observation in Ref. [51], and g is a function that can have both oscillating and non-oscillating dependence on $p \cdot x$. For large enough $|x|$, the exponential decay should suppress the correlation and make it or its extremes decrease monotonically in

magnitude.

Note that after we match the hybrid scheme matrix elements to $\overline{\text{MS}}$, the renormalon ambiguity in the Wilson line mass, $m_0^{\overline{\text{MS}}}$, is subtracted out, so the matched result should exhibit an asymptotic behavior that goes as $e^{-(\bar{\Lambda}-m_0^{\overline{\text{MS}}})|z|}$ at large z . Therefore, the sign of $(\bar{\Lambda}-m_0^{\overline{\text{MS}}})$ becomes crucial in determining whether it is exponentially decaying or growing.

In QCD sum rule calculations, the result is $\bar{\Lambda} = 0.4 - 0.6$ GeV from phenomenology, while $m_0^{\overline{\text{MS}}}$ is expected to be $0.1 - 0.2$ GeV [52], so $\bar{\Lambda} - m_0^{\overline{\text{MS}}} = 0.2 - 0.5$ GeV. Since the quarks have heavier-than-physical masses in our lattice calculation, one should expect a larger $\bar{\Lambda}$, so it is very likely that $\bar{\Lambda} - m_0^{\overline{\text{MS}}}$ still remains positive. After all, this can be always put to test on the $P^z = 0$ matrix elements since $\bar{\Lambda} - m_0^{\overline{\text{MS}}}$ is a Lorentz-invariant quantity.

2. Extrapolation and FT

If z_L is large enough for the correlation $\tilde{h}(z)$ to reach the asymptotic region, then an extrapolation that encodes the exponential decay behavior we derived in App. B 1 should lead to reliable FT for moderate-to-large x . To be more precise, there is a rigorous upper bound for the uncertainty of FT which decreases with x .

To prove the above statement, let us consider extrapolation based on the general model

$$\tilde{h}(\lambda) = e^{-c|\lambda-\lambda_L|}g(\lambda), \quad (\text{B15})$$

where $g(\lambda_L) = \tilde{h}(\lambda_L)$, and $c = m_{\text{eff}}/P^z$ with m_{eff} being the effective mass for the exponential decay. Motivated by QCD sum rule results, we expect $m_{\text{eff}} \sim 0.2 - 0.5$ GeV, which can be larger since we have used heavier-than-physical quark masses. Therefore, for $P^z \sim 2.0$ GeV in the current work, we should have $c \sim 0.10 - 0.25$ or higher.

Now let us compare two extrapolations h_1 and h_2 with different g_1 and g_2 . The difference between the two extrapolations,

$$\delta\tilde{h}(\lambda) \equiv \tilde{h}_1(\lambda) - \tilde{h}_2(\lambda), \quad (\text{B16})$$

should satisfy $\delta\tilde{h}(\lambda_L) = 0$ and $\delta\tilde{h}(\infty) = 0$. The difference in the FT with extrapolation is therefore

$$\delta\tilde{f}(x) = \int_{\lambda_L}^{\infty} \frac{d\lambda}{\pi} \delta\tilde{h}(\lambda) \cos(x\lambda). \quad (\text{B17})$$

If we can approximate $\delta\tilde{h}(\lambda)$ as a flat curve within one period of the oscillatory function $\cos(x\lambda)$, then the integral in that region vanishes. This condition can be satisfied if $|\delta\tilde{h}'(\lambda)| \ll x$, which should be reached very quickly due to the exponential suppression at large λ . For each x , there should be a minimal integer N_x which satisfies

$|\delta\tilde{h}'(\lambda_L + N_x 2\pi/x)| \ll x$, so that we can approximate $\delta\tilde{f}(x)$ as

$$\delta\tilde{f}(x) \approx \int_{\lambda_L}^{\lambda_L + N_x \frac{2\pi}{x}} \frac{d\lambda}{\pi} \delta\tilde{h}(\lambda) \cos(x\lambda). \quad (\text{B18})$$

Since $\delta\tilde{h}(\lambda_L) = 0$ and $\delta\tilde{h}(\infty) = 0$, there must be at least one extremum of $\delta\tilde{h}(\lambda)$ for $\lambda_L < \lambda < \infty$, so we have the inequality

$$\begin{aligned} |\delta\tilde{f}(x)| &< \int_{\lambda_L}^{\lambda_L + N_x \frac{2\pi}{x}} \frac{d\lambda}{\pi} |\delta\tilde{h}(\lambda)| |\cos(x\lambda)| \\ &< N_x |\delta\tilde{h}(\lambda)|_{\text{max}} \int_{\lambda_L}^{\lambda_L + \frac{2\pi}{x}} \frac{d\lambda}{\pi} |\cos(x\lambda)| \\ &= \frac{4N_x |\delta\tilde{h}(\lambda)|_{\text{max}}}{\pi x} \lesssim \frac{4N_x |\tilde{h}(\lambda_L)|}{\pi x}. \end{aligned} \quad (\text{B19})$$

According to our estimate of $\bar{\Lambda} - m_0^{\overline{\text{MS}}}$, $c \gtrsim 0.1$ at $P^z \sim 2$ GeV, so

$$e^{-cN_x(2\pi)/x} \lesssim e^{-0.6N_x/x}, \quad (\text{B20})$$

and $N_x \sim \mathcal{O}(1)$ should be sufficient to satisfy $|\delta\tilde{h}'(\lambda_L + N_x 2\pi/x)| \ll x$ with $0 < x < 1$. Therefore, in Eq. (B19) we demonstrate that there is an upper bound for the model uncertainty in the FT with exponential extrapolation, which decreases in x . The error is also proportional to $|\delta\tilde{h}(\lambda)|_{\text{max}}$ which can be much smaller than $|\tilde{h}(\lambda_L)|$ that is already close to zero. If $h(\lambda_L) = 0.1$, $|\delta\tilde{h}(\lambda)|_{\text{max}} = 0.05$, and $N_x = 1$, then we have

$$|\delta\tilde{f}(x)| < \frac{0.07}{x}, \quad (\text{B21})$$

which is less than 0.15 at $x = 0.5$ and around 15% of the central value of the qPDF as we obtain below. It is worth pointing out that our estimate of the upper bound in Eq. (B19) can be highly overestimated, as $\delta\tilde{h}(\lambda)$ has an oscillation from $\cos(\lambda)$ and $\sin(\lambda)$ which are out of pace with $\cos(x\lambda)$ for $0 < x < 1$, and $|\delta\tilde{h}(\lambda)|_{\text{max}}$ could be much smaller than $|\tilde{h}(\lambda_L)|$ and at a sharp peak within $\lambda_L < \lambda < \lambda_L + N_x 2\pi/x$.

Therefore, the FT with exponential extrapolation is under control for moderate and large x . When $\tilde{h}(\lambda_L)$ is small enough, the model uncertainty from the extrapolation can be controlled to be much smaller than the other systematic uncertainties which are about 10% – 20% in this work.

It is worth to compare with the extrapolation error when the correlation function decreases algebraically as $1/|\lambda|^d$, which corresponds to the generic model

$$\tilde{h}(\lambda) = \left(\frac{\lambda_L}{\lambda}\right)^d g(\lambda). \quad (\text{B22})$$

Suppose we truncate at $\lambda_L = 10$, then

$$\left(\frac{\lambda_L}{\lambda_L + N_x 2\pi/x}\right)^d \sim (1 + 0.6N_x/x)^{-d}. \quad (\text{B23})$$

The power d is related to the small- x behavior of the PDF. If we parameterize the PDF as $\sim x^a(1-x)^b$, then with LO matching one can derive that $d = \min\{1+a, 1+b\}$ [19], which is $\mathcal{O}(1)$ empirically. Therefore, it will take $N_x \gg 1$ for the factor in Eq. (B23) to decrease sufficiently to satisfy the condition $|\delta\tilde{h}'(\lambda_L + N_x 2\pi/x)| \ll x$. As a result, the uncertainty in the FT is of orders of magnitude larger than that of extrapolation with exponential decay.

To test our claim of controlled FT error with exponential decay, we choose a particular model

$$\tilde{h}(\lambda) = \tilde{h}(\lambda_L) \left(\frac{\lambda_L}{\lambda}\right)^d e^{-c|\lambda-\lambda_L|}. \quad (\text{B24})$$

Suppose that the extrapolation is done at $\lambda_L = 10$ with $\tilde{h}(\lambda_L) = 0.15$, and the parameters c and d are fitted with errors δc and δd , then we analytically FT the extrapolated result to the x -space, and calculate its error using

$$\delta\tilde{f}(x, c, d) = \sqrt{\left(\frac{\partial\tilde{f}}{\partial c}\right)^2 \delta c^2 + \left(\frac{\partial\tilde{f}}{\partial d}\right)^2 \delta d^2}. \quad (\text{B25})$$

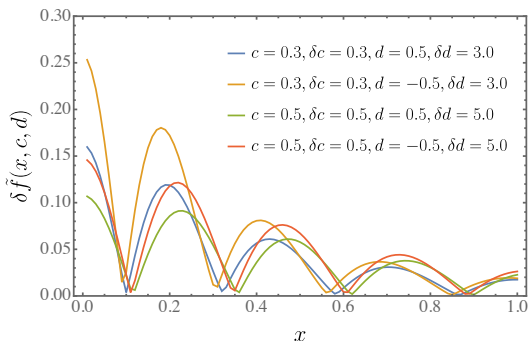


FIG. 9. Estimate of error in the FT with extrapolation using the model in Eq. (B24).

In Fig. 9, we plot the extrapolation error against x . We have chosen different central values of the parameters c and d and fairly large uncertainties in them. The parameter d cannot have a large negative value, otherwise it would make $\tilde{h}(\lambda)$ grow beyond λ_L . In most of the scenarios considered, the error is $\lesssim 0.1$ for $x > 0.1$. As we shall see below, the actual extrapolation error is much smaller than this estimate and thus negligible when compared to the other systematic errors.

In the following, we perform the extrapolation with four different models. The extrapolation is carried out on each bootstrap sample by a minimal-square fit. For each P^z , we truncate $\tilde{h}(z)$ at the largest z , $z_{>0}$, where the central value of $\tilde{h}(z)$ remains positive, and choose $z_{\max} = \{z_{>0} - 2a, z_{>0} - a, z_{>0}\}$ to estimate the truncation error. The range of z used to fit the parameters is $z_{\min} \leq z \leq z_{\max}$ where z_{\min} satisfies $\tilde{h}(z_{\min}) < 0.2$. The continuity

n_z	z_L/a	
	$a = 0.04$ fm	$a = 0.06$ fm
1	{29, 30, 31}	N/A
2	{26, 27, 28}	{19, 20, 21}
3	{19, 20, 21}	{16, 17, 18}
4	{24, 25, 26}	{14, 15, 16}
5	{21, 22, 23}	{15, 16, 17}

TABLE I. Choices of z_L for the extrapolations.

condition between data and model was imposed in the middle point of the fit range, namely z_L , which is listed in Table I. The extrapolation models are:

Exponential decay model, or “model-exp”. The model for extrapolation is

$$A \frac{e^{-m_{\text{eff}}|z|}}{|\lambda|^d}. \quad (\text{B26})$$

We have tried to fit m_{eff} from the same range of z for $P^z = 0$ matrix elements with a similar form, $Ae^{-m_{\text{eff}}|z|}/|z|^d$, and found that m_{eff} is around 0.1 GeV, about the same scale as the phenomenological estimate. For the $P^z \neq 0$ matrix elements, we do not fix m_{eff} , but constrain it with a prior $m_{\text{eff}} \geq m_{\min}$. To test the dependence on this prior condition, we have set $m_{\min} = \{0, 0.1, 0.2\}$ GeV. Besides, we also impose $A > 0$ and $d > 0$ to ensure that the extrapolated result is positive and decreases in λ .

Power-law decay model, or “model-pow”. The model is defined by setting $m_{\text{eff}} = 0$ in model-exp. As the $P^z \rightarrow \infty$ limit of model-exp, model-pow can be used to give a coarse estimate of the significance of higher-twist effects, although its FT error is not well under control as we discussed above. We impose the conditions $A, d > 0$ so that the fitted results decrease to zero as $\lambda \rightarrow \infty$.

Two-parameter model with exponential decay, or “model-2p-exp”. As we can see from Fig. 1, the matrix elements at $\lambda_L \sim 6 - 10$ do not show a clear exponential decay, although they can be fitted by the latter with $\chi^2/d.o.f < 1$ due to the large errors. This may indicate that there is oscillation in $\tilde{h}(\lambda)$. To incorporate such dependence, we first ignore the higher-twist contributions, and assume that the qPDF is the same as the PDF which is parameterized as

$$f_v(x; a, b) = \frac{\Gamma(2+a+b)}{\Gamma(1+a)\Gamma(1+b)} |x|^a (1-|x|)^b \times \theta(|x|)\theta(1-|x|). \quad (\text{B27})$$

By doing an inverse FT into the λ -space, the asymptotic form of $h_{2p}(\lambda)$ at large λ reads,

$$\tilde{h}_{2p}(\lambda) = A \text{Re} \left[\frac{\Gamma(1+a)}{(-i|\lambda|)^{a+1}} + e^{i\lambda} \frac{\Gamma(1+b)}{(i|\lambda|)^{b+1}} \right]. \quad (\text{B28})$$

Then we multiply $\tilde{h}_{2p}(\lambda)$ with an exponential decay factor as our model for extrapolation,

$$\tilde{h}_{2p\text{-exp}} = \tilde{h}_{2p}(\lambda) e^{-m_{\text{eff}}(z-z_L)}. \quad (\text{B29})$$

Two-parameter model, or “model-2p”. Again, we ignore the exponential decay and use \tilde{h}_{2p} as the extrapolation model, which can help us estimate the significance of higher-twist effects.

In Fig. 10 we compare the FT with different z_L for extrapolation with model-exp and condition $m_{\text{eff}} > 0.1$ GeV. Except for very small x , the results are consistent, and those at smaller z_L have smaller errors because the error of the matrix element grows with z . Therefore, for the rest of our analysis, we simply use the largest z_L for each P^z .

In Fig. 11 we show the extrapolations with different models, which have noticeable differences at $\lambda > \lambda_L$. In Fig. 12 we compare the FT with different extrapolation models as well as with the discrete FT (DFT). As we can see, the DFT introduces unphysical oscillation in the qPDF which is due to the truncation of $\tilde{h}(\lambda)$ at λ_L . In contrast, the extrapolations are free of such oscillation, and different models yield consistent qPDFs at moderate and large x , though they differ significantly at small x . We notice that the qPDF from model-2p extrapolation still has slight oscillations despite its agreement with the others, because the extrapolated result decays too slowly at $\lambda > \lambda_L$. As expected, the models with exponential decay lead to regular qPDFs at $x = 0$, whereas model-pow and model-2p give divergent qPDFs as $x \rightarrow 0$.

Based on the above results, we use model-exp with $m_{\text{eff}} > 0.1$ GeV for the FT in our following analysis. To have a coarse estimate of the uncertainties from extrapolation model and higher-twist contributions, we look into the difference between final PDFs matched from qPDFs with model-exp and model-pow extrapolations.

Recall that although the hybrid-scheme matrix elements $\tilde{h}(\lambda, \lambda_S, P^z)$ should be RG invariant, they can still depend on μ due to the fixed-order Wilson coefficients used in the matching between lattice and $\overline{\text{MS}}$ schemes. In Fig. 13, we compare the qPDFs which are FTs of $\tilde{h}(\lambda, \lambda_S, P^z, \mu, a)$ obtained at $a = 0.04$ fm with C_0^{NLO} and C_0^{NNLO} . We choose $\mu = 1.0$ GeV for C_0^{NLO} and $\mu = 2.0$ GeV for C_0^{NNLO} as the *ansatz* in Eq. (A11) appear to best describe the lattice matrix elements according to Fig. 8 at these scales. The results are almost identical to each other, which shows that the renormalon-inspired model with fixed-order Wilson coefficient can indeed describe the data within a specific window of μ . At NLO, smaller μ is favored as $\alpha_s(\mu)$ is larger so that the renormalon effects become important at lower orders. In Fig. 14 we show the μ -dependence of the qPDFs from NLO- and NNLO-matched $\tilde{h}(\lambda, \lambda_S, P^z, \mu, a)$. As one can see, the results have mild dependence on μ which becomes more significant at lower scales. One can expect that the uncertainty from scale variation will also be larger in this region.

Appendix C: Perturbative matching

In this section we perform the perturbative matching to the qPDF. Recall that Eq. (7) relates the qPDF to the PDF,

$$f_v(x, \mu) = \int_{-\infty}^{\infty} \frac{dy}{|y|} C^{-1}\left(\frac{x}{y}, \frac{\mu}{yP^z}, |y|\lambda_S\right) \tilde{f}_v(y, z_S, P^z) + \mathcal{O}\left(\frac{\Lambda_{\text{QCD}}^2}{(xP^z)^2}, \frac{\Lambda_{\text{QCD}}^2}{((1-x)P^z)^2}\right). \quad (\text{C1})$$

The matching kernel C can be expanded to $O(\alpha_s)$ as

$$C\left(\frac{x}{y}, \frac{\mu}{yP^z}, |y|\lambda_S\right) = \delta\left(\frac{x}{y} - 1\right) + \alpha_s C^{(1)}\left(\frac{x}{y}, \frac{\mu}{yP^z}, |y|\lambda_S\right) + \alpha_s^2 C^{(2)}\left(\frac{x}{y}, \frac{\mu}{yP^z}, |y|\lambda_S\right) + \mathcal{O}(\alpha_s^3). \quad (\text{C2})$$

The inverse matching kernel C^{-1} can be obtained by solving

$$\int \frac{dz}{|z|} C^{-1}\left(\frac{x}{z}, \frac{\mu}{zP^z}, |z|\lambda_S\right) C\left(\frac{z}{y}, \frac{\mu}{yP^z}, |y|\lambda_S\right) = \delta\left(\frac{x}{y} - 1\right) \quad (\text{C3})$$

order by order in α_s [55], and the result is

$$C\left(\frac{x}{y}, \frac{\mu}{yP^z}, |y|\lambda_S\right) = \delta\left(\frac{x}{y} - 1\right) - \alpha_s C^{(1)}\left(\frac{x}{y}, \frac{\mu}{yP^z}, |y|\lambda_S\right) + \alpha_s^2 \int \frac{dz}{|z|} C^{(1)}\left(\frac{x}{z}, \frac{\mu}{zP^z}, |z|\lambda_S\right) C^{(1)}\left(\frac{z}{y}, \frac{\mu}{yP^z}, |y|\lambda_S\right) - \alpha_s^2 C^{(2)}\left(\frac{x}{y}, \frac{\mu}{yP^z}, |y|\lambda_S\right) + \mathcal{O}(\alpha_s^3). \quad (\text{C4})$$

It has been shown in Ref. [55] that the inverse matching coefficient satisfies the correct RG and P^z -evolution equations.

1. Numerical implementation of matching

Since in the asymptotic regions,

$$\lim_{y \rightarrow \infty} C\left(\frac{x}{y}\right) \rightarrow \text{finite}, \quad \lim_{y \rightarrow 0} C\left(\frac{x}{y}\right) \propto \frac{y^2}{x^2}, \quad (\text{C5})$$

and

$$C\left(\frac{x}{y}\right) \equiv C_r\left(\frac{x}{y}\right) - \delta\left(\frac{x}{y} - 1\right) \int_{-\infty}^{\infty} dy' C_r(y') \quad (\text{C6})$$

is a plus function (with “ r ” denotes the $x \neq y$ part) that regulates the singularity at $y = x$, the convolution integral in Eq. (C1) is convergent and insensitive to the

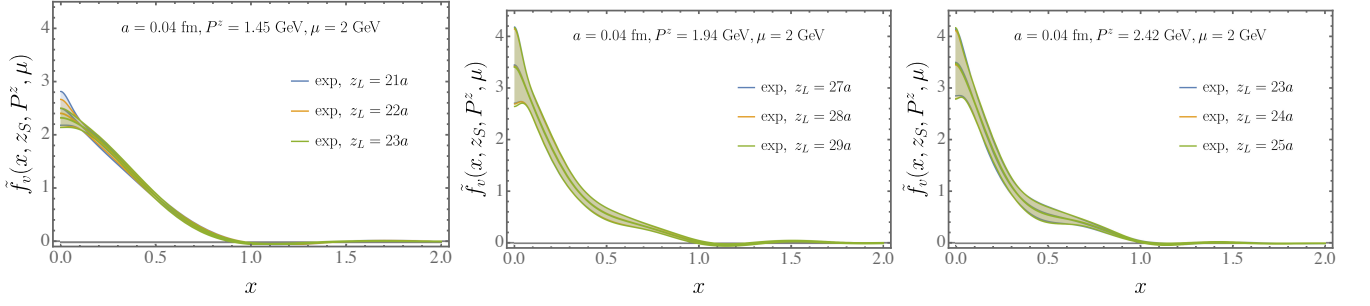


FIG. 10. FT with different z_L for model-exp extrapolation (with prior $m_{\text{eff}} > 0.1$ GeV) of the NNLO-matched $\tilde{h}(\lambda, \lambda_S, P^z, \mu, a)$ at $z_S = 0.24$ fm.

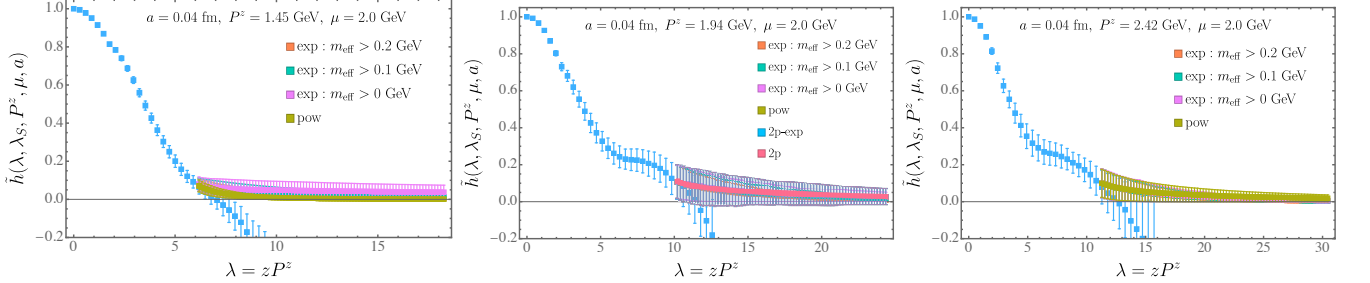


FIG. 11. Extrapolation with different models for the NNLO-matched $\tilde{h}(\lambda, \lambda_S, P^z, \mu, a)$. At $P^z = 1.94$ GeV, we have added the comparison with the 2p-exp and 2p models.

cutoffs for $y \rightarrow 0, x, \infty$, as long as the qPDF is integrable. Therefore, we are able to evaluate the integral numerically within a finite range of y with a target precision.

The numerical integration in Eq. (7) is time consuming, especially when we have to perform the matching for the qPDF on each bootstrap sample. Therefore, to speed up the matching procedure, we discretize the integral in Eq. (7) and reexpress it as multiplication of a matching matrix and the qPDF vector. In our implementation, our integration domain is $-2.0 < y < 2.0$ discretized with a step size $\delta y = 0.001$. Since the qPDF falls very close to zero at $|y| = 2.0$, the corresponding uncertainty is negligible as we have varied the truncation point. Note that the matching coefficient is a plus function, the step size δy also serves as a soft cutoff for the singularity near $|x/y| = 1$ in the plus functions. To test how well the matrix multiplication can reproduce the exact numerical integration, we compare the NLO corrections to the qPDF from one bootstrap sample using the two methods in Fig. 15. With our current step size, the results are almost identical for x as small as 0.01.

Moreover, to test the reliability of our inverse matching coefficient, which is obtained through expansion in α_s , we compare it to direct matrix inversion. To be specific, we construct a square matching matrix C in x and y with $x, y \in [-2, 2]$, which is asymmetric but has dominant diagonal elements, and then invert it to obtain the inverse matching matrix C^{-1} . At small α_s , the matrix C can be schematically expressed as

$$C = \mathcal{I} + \mathcal{E}, \quad (\text{C7})$$

where \mathcal{I} is an identity matrix, whereas \mathcal{E} is $\mathcal{O}(\alpha_s)$, so that its inverse can be expanded as

$$C^{-1} = \mathcal{I} - \mathcal{E} + \mathcal{E}^2 - \mathcal{E}^3 + \dots \quad (\text{C8})$$

In Fig. 16a we first test the convergence of the solution in Eq. (C8) for the NLO matching matrix. By expanding the solution to order n , we calculate the NLO matching correction to a qPDF sample, and then compare it to the result from direct matrix inversion. Since our main purpose is to compare the two inversion methods, we increase the step size to $\delta y = 0.01$ to reduce the computing time regardless the accuracy of numerical integration. We find that by increasing n , the expansion method gradually converges to direct inversion, as expected. Of course, in perturbation theory, we should calculate the matching coefficient to n -loop accuracy for consistency, for α_s is the actual power-counting parameter.

In Fig. 16b we compare the NLO and NNLO matching corrections to a qPDF sample using direct matrix inversion and the α_s -expansion methods. The results are basically consistent with each other for almost the entire range of $x \in (0, 1)$, except for small deviations. This is because direct matrix inversion includes all-order terms in α_s , and the deviations reflect the size of higher-order effects, whose smallness shows that the perturbation series is convergent. With our current two-loop accuracy, we adopt the α_s -expansion method.

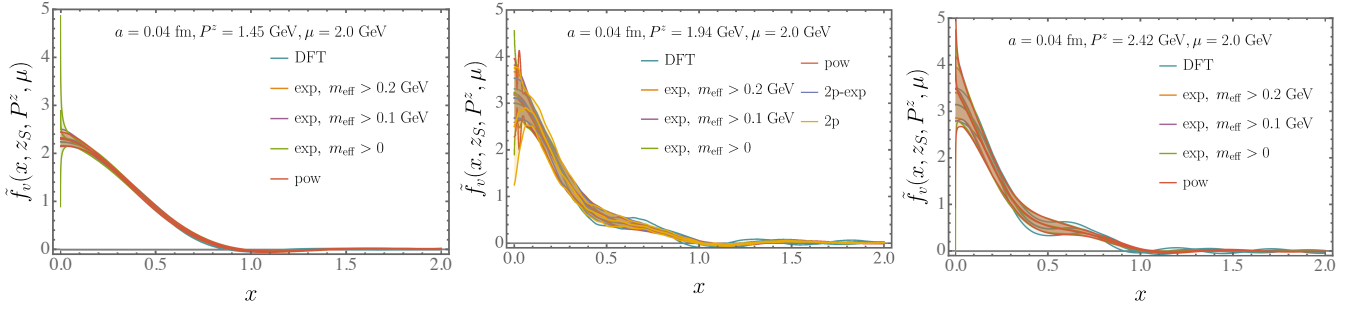


FIG. 12. Comparison of DFT and FT with different extrapolation models for the NNLO-matched $\tilde{h}(\lambda, \lambda_S, P^z, \mu, a)$ at $z_S = 0.24$ fm. At $P^z = 1.94$ GeV, we have added the comparison with the 2p-exp and 2p models.

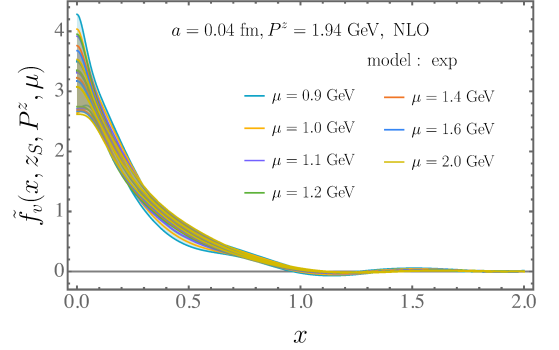
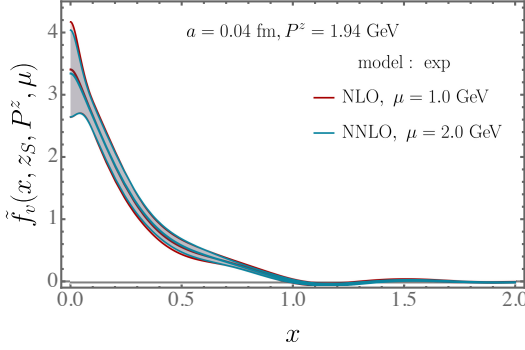
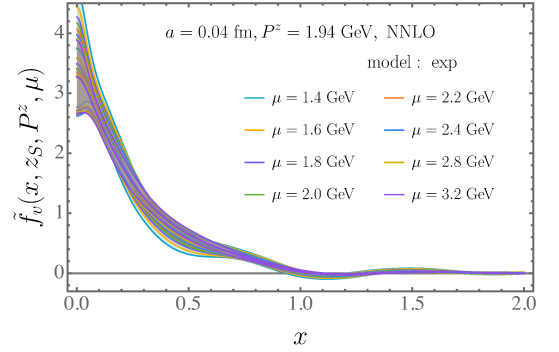


FIG. 13. Comparison of the qPDF with model-exp extrapolation (with $m_{\text{eff}} > 0.1$ GeV) of the NLO- and NNLO-matched $\tilde{h}(\lambda, \lambda_S, P^z, \mu, a)$ at $z_S = 0.24$ fm and $z_L = 26a$. The choices of μ are based on where the renormalon model best describes the matrix elements.



2. Perturbative convergence

In Fig. 17 we show the matched results for the PDF from the qPDF obtained from model-exp extrapolation (with $m_{\text{eff}} > 0.1$ GeV) of the NNLO-matched $\tilde{h}(\lambda, \lambda_S, P^z, \mu, a)$. As one can see, the NNLO correction is generally smaller than the NLO correction for moderate x , which indicates good perturbative convergence. Near the end-point regions, the NLO and NNLO corrections become larger than 50%, which suggests that higher-order corrections or resummation effects become important.

To see whether the NNLO matching reduces the uncertainty from scale variation, we match qPDFs at different μ to the corresponding PDFs, and then use DGLAP equation to evolve the results to $\mu = 2.0$ GeV. We use NLO matching coefficient and LO DGLAP evolution kernel for the qPDF obtained from the NLO-matched $\tilde{h}(\lambda, \lambda_S, P^z, \mu, a)$, and NNLO matching coefficient and NLO DGLAP evolution kernel for the qPDF obtained from the NNLO-matched $\tilde{h}(\lambda, \lambda_S, P^z, \mu, a)$. The NLO

FIG. 14. Comparison of the qPDF at different μ with model-exp extrapolation of the NLO- and NNLO-matched $\tilde{h}(\lambda, \lambda_S, P^z, \mu, a)$.

DGLAP evolution formula takes the following form,

$$f_v(x, \mu) = f_v(x, \mu_0) + \frac{\alpha_s(\mu_0)t}{2\pi} \int_x^1 \frac{dy}{|y|} P_{qq}^{(0)}\left(\frac{x}{y}\right) f_v(y, \mu_0) + \left(\frac{\alpha_s(\mu_0)t}{2\pi}\right)^2 \int_x^1 \frac{dy}{|y|} \left[P_{qq}^{V(1)} + \frac{1}{2} P_{qq}^{(0)} \otimes P_{qq}^{(0)} - \frac{\beta_0}{2} P_{qq}^{(0)} \right] \left(\frac{x}{y}\right) f_v(y, \mu_0), \quad (\text{C10}) \quad (\text{C9})$$

where $t = \ln(\mu^2/\mu_0^2)$, $\beta_0 = (11C_A - 2n_f)/6$, $P_{qq}^{(0)}$ is the LO splitting kernel, and $P_{qq}^{V(1)}$ is the NLO splitting kernel [70] for the valence quark PDF.

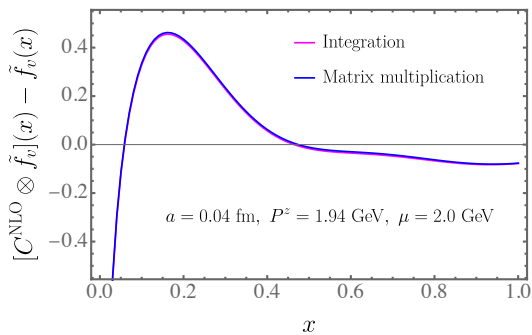


FIG. 15. Comparison of matrix multiplication to direct numerical integration for the NLO matching correction to one qPDF sample.

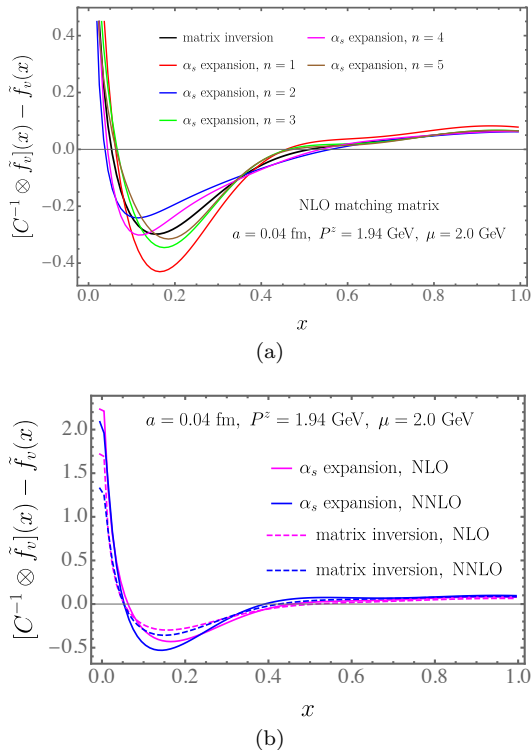


FIG. 16. (a) Comparison of the NLO matching correction to the qPDF with matrix inversion and the expansion in Eq. (C8) to order n . (b) Comparison of NLO and NNLO matching corrections to the qPDF from direct matrix inversion and the α_s -expansion in Eq. (C4).

Since there are only a few common μ values for the NLO- and NNLO- matched $\tilde{h}(\lambda, \lambda_s, P^z, \mu, a)$, we choose $\mu = 1.4$ and 2.0 GeV for our comparison. In Fig. 18 we show the scale variation of the PDFs from NLO and NNLO matching, where only the central values are plotted for our purpose. As one can see, the NNLO matching correction significantly reduces the uncertainty for $x \lesssim 0.4$ at NLO, while for $x \gtrsim 0.4$ the NNLO uncertainty band is still about a factor of one half of the NLO case. Therefore, the NNLO matching does indeed improve the perturbation theory uncertainty.

Finally, for the NNLO matching we vary $\mu = 2.0$ GeV by a factor of $\sqrt{2}$ and $1/\sqrt{2}$, and then use NLO DGLAP equation to evolve the matched results to $\mu = 2.0$ GeV, whose central values are shown in Fig. 19. As one can see, there is virtually no difference between choosing $\mu = 2.0$ and 2.8 GeV as the factorization scale, but the lower choice of $\mu = 1.4$ GeV does introduce larger uncertainty mainly because α_s becomes too large. Nevertheless, such uncertainty is still quite small compared to the other systematics.

3. Dependence on P^z , a and extrapolation model

In Fig. 20 we show the P^z -dependence of the PDF with NNLO matching correction. We find that despite the considerable differences between the qPDFs at $P^z \leq 1.45$ GeV and those at $P^z \geq 1.94$ GeV, the matching corrections bring the final results closer, which shows the effectiveness of LaMET. Note that the matching drives the qPDF closer to the smaller x region, so the error bands of the PDFs also shrink after matching as they are contributed from the larger x region. Moreover, we find that the PDFs start to converge at $P^z \geq 1.29$ GeV, which corresponds to a boost factor of ~ 4 . As P^z increases, the results become smaller as $x \rightarrow 1$, which agrees with our expectation that large momentum suppresses the higher-twist contributions. It is worth mentioning that both the P^z -dependence and matching correction appear to be small for x as low as 0.05 , which hints that the power correction and resummation effects are less severe than our naive estimate through power counting.

In Fig. 21 we compare the PDFs matched from the qPDFs with model-exp (with $m_{\text{eff}} > 0.1$ GeV) and model-pow extrapolations. For $a = 0.04$ fm and $P^z = 1.94$ GeV, we also added comparison to the model-2p-exp and model-2p extrapolations. Despite the differences between the qPDFs at small x , the matched results are almost identical even at the smallest x shown in the plot. Again, this is the outcome of the PDF receiving contributions from the qPDF at larger x through matching, which suggests that the extrapolation error can still be under control for x as small as ~ 0.01 . Note that the result from model-2p also shows agreement, but it includes slight oscillations in the x -space, because the extrapolated $\tilde{h}(\lambda)$ decays too slowly in the coordinate space. Therefore, in the region where other systematic errors are under control, the difference between model-exp and other extrapolations is negligible, and we will use the model-exp extrapolation to obtain the final results.

Appendix D: Final results

The central value of our final result is obtained from the qPDF at $a = 0.04$ fm, $z_S = 0.24$ fm, $z_L = 0.92$ fm, $\mu = 2.0$ GeV and $P^z = 2.42$ GeV with exponential ex-

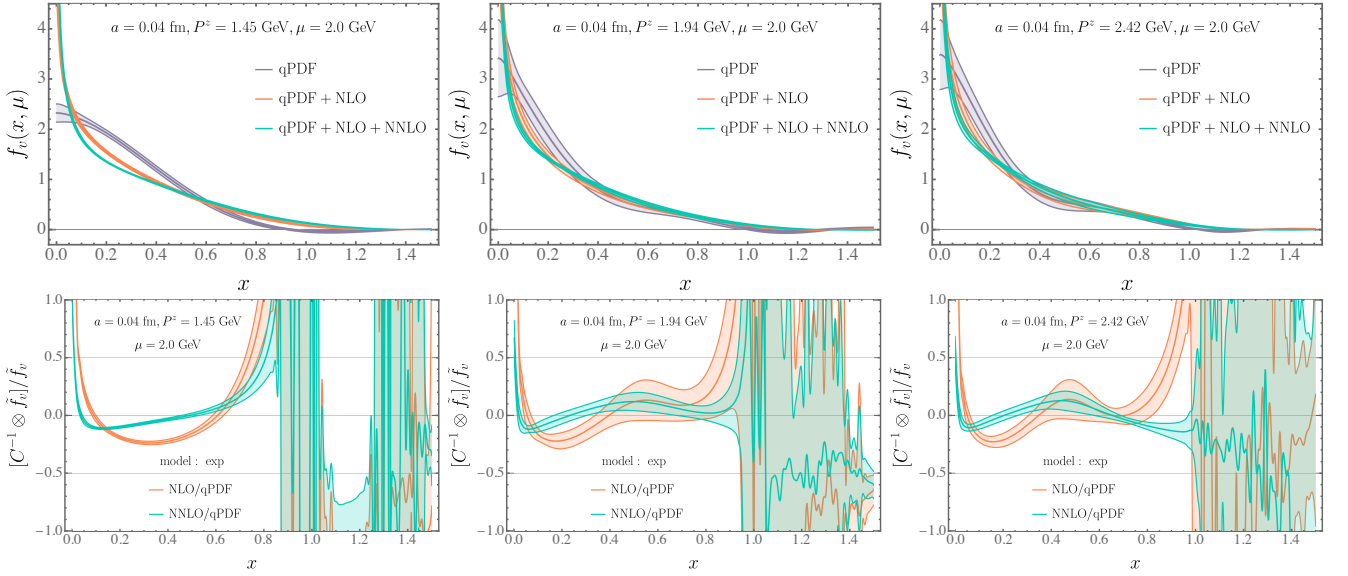


FIG. 17. Upper row: the PDFs from NLO and NNLO matching corrections are compared to the qPDF (or LO PDF), which is obtained from model-exp (with $m_{\text{eff}} > 0.1$ GeV) extrapolation of the NNLO-matched $\tilde{h}(\lambda, \lambda_S, P^z, \mu, a)$. Lower row: the ratio of NLO and NNLO corrections to the qPDF.

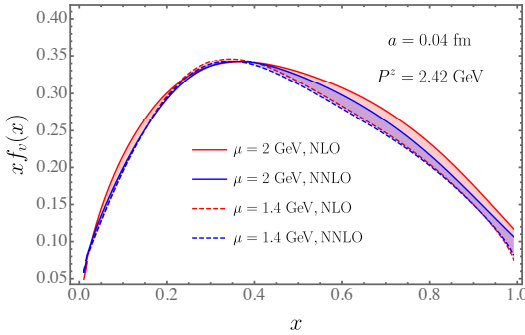


FIG. 18. Comparison of the PDFs at different μ obtained from the NLO- and NNLO-matched $\tilde{h}(\lambda, \lambda_S, P^z, \mu, a)$.

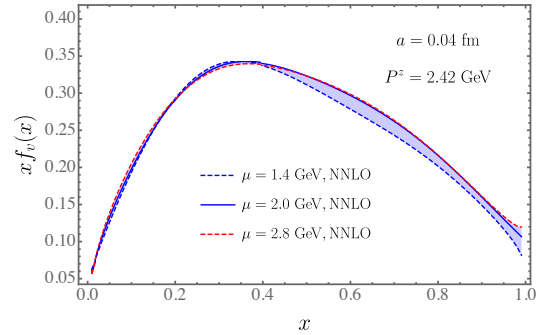


FIG. 19. Comparison of the PDFs obtained from NNLO matching of the qPDFs at different μ and NLO DGLAP evolution to $\mu = 2.0$ GeV.

trapolation ($m_{\text{eff}} > 0.1$ GeV) and NNLO matching. The error from variation of the factorization scale is obtained by repeating the same procedure for $\mu = 1.4$ and 2.8 GeV and evolving the matched results to $\mu = 2.0$ GeV with the NLO DGLAP equation, as shown in Fig. 19, where let the error band cover all the data sets from the three different factorization scales.

In order to obtain a target precision of 10%, we aim to control the relative $O(\alpha_s^3)$ matching correction at $\mu = 2.0$ GeV be smaller than 5%. By assuming that the perturbation series grows geometrically, it means that the relative NLO correction should be less than $\sqrt[3]{5\%} = 37\%$ and the relative NNLO correction less than 14%. By comparing to Fig. 17, it means that we should exclude the regions $x < 0.03$ and $x > 0.88$.

To estimate the size of the power corrections, we fit the PDFs obtained at $a = 0.04$ fm, $P^z = \{1.45, 1.94, 2.42\}$ GeV and $a = 0.06$ fm, $P^z = \{1.72, 2.15\}$ GeV to the

ansatz $f_v(x) + \alpha(x)/P_z^2$ for each fixed x , and show the size of the power correction term in Fig. 22. At $P^z = 2.42$ GeV, we find that the absolute value of the power correction diverges at very small x , as expected, but its relative size $\alpha(x)/[P_z^2 f_v(x)]$ remains finite because the PDF also diverges. On the contrary, $\alpha(x)/[P_z^2 f_v(x)]$ starts to grow as $x \rightarrow 1$. According to our estimate, $\alpha(x)/[P_z^2 f_v(x)] \lesssim 0.1$ for $0.01 < x < 0.80$ and $\alpha(x)/[P_z^2 f_v(x)] \lesssim 0.05$ for $0.01 < x < 0.70$. According to Fig. 21, the qPDF from power-law extrapolation leads to almost identical PDF after the matching correction for x as small as 0.01. Our explanation is that the matching correction drives the qPDF to the smaller x region, so the PDF at a given x receives contributions from the larger- x region of the qPDF which has less P^z dependence. Although there are logarithms of $\mu/(xP^z)$ in the matching coefficient which become large at small x , they are always multiplied by

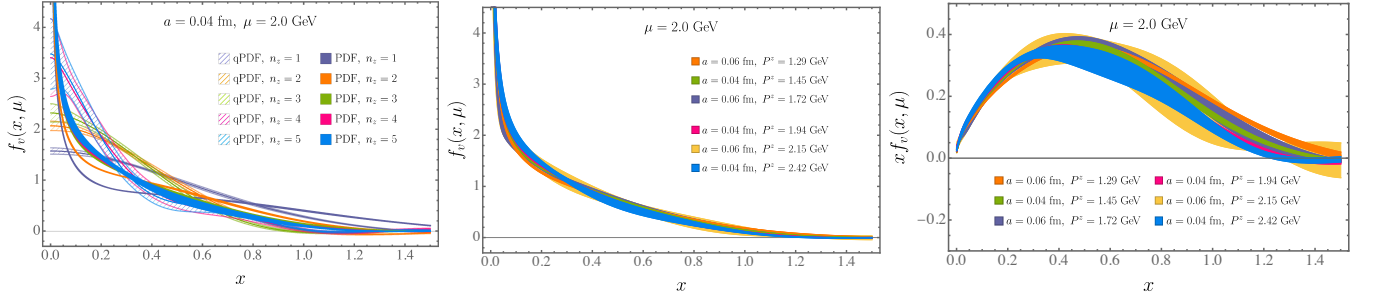


FIG. 20. The PDFs from NNLO matching of the qPDFs at different P^z , which is obtained from model-exp extrapolation of the NNLO-matched $\tilde{h}(\lambda, \lambda_S, P^z, \mu, a)$.

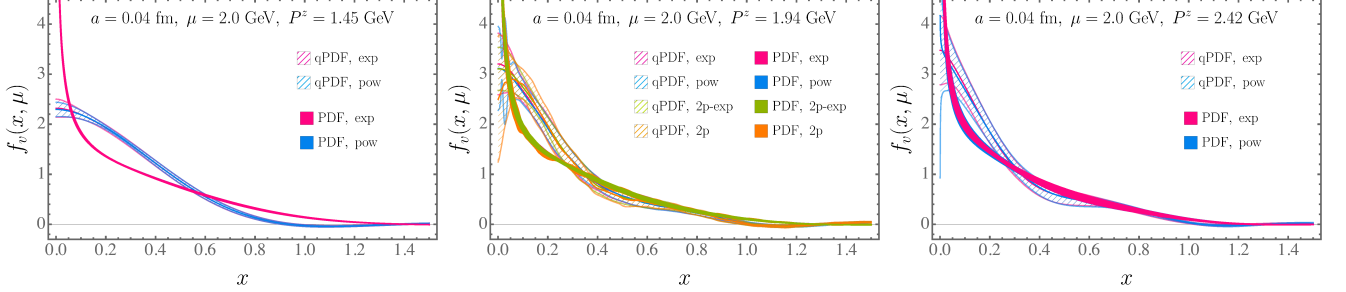


FIG. 21. Comparison of the final results from qPDFs obtained by different model extrapolations for the FT.

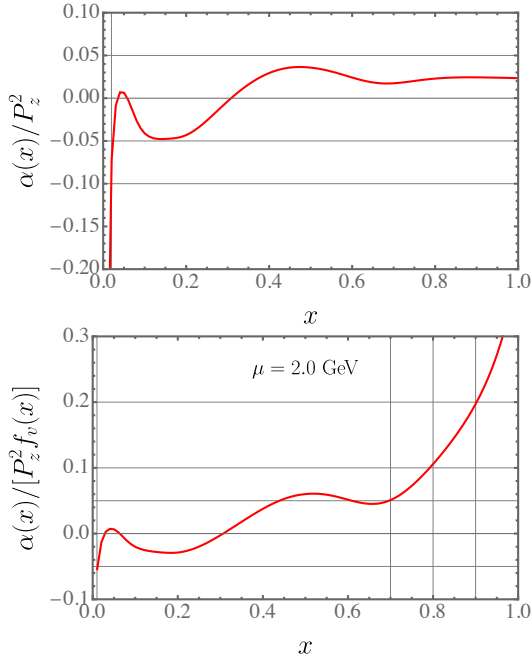


FIG. 22. Estimate of the size of power correction $\alpha(x)/P_z^2$ (upper panel) and its relative size to the qPDF $\tilde{f}_v(x, P^z = 2.42 \text{ GeV})$ (lower panel).

the DGLAP splitting function, which when convoluted with the qPDF always drives the result to smaller x , thus the perturbative correction remains small even at $x = 0.03$.

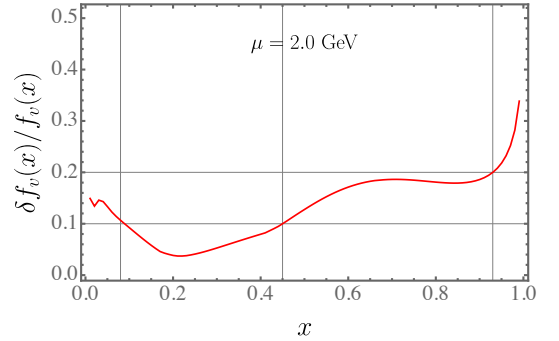


FIG. 23. Statistical and systematic uncertainty of the PDF obtained from the qPDF at $a = 0.04 \text{ fm}$ and $P^z = 2.42 \text{ GeV}$.

In Fig. 23 we show uncertainty of the PDF, $\delta f_v(x)/f_v(x)$, where $\delta f_v(x)$ includes both statistical and scale-variation errors. The uncertainty is $\leq 20\%$ for $0.01 \leq x \leq 0.93$, as $x = 0.01$ is the smallest x that we show in the plot, and $\leq 10\%$ for $0.08 \leq x \leq 0.45$.

Therefore, by combining the estimates of power correction, higher-order perturbative correction, statistical and scale-variation errors, we determine the PDF at $0.03 \lesssim x \lesssim 0.80$ with $\leq 20\%$ uncertainty and at $0.08 \lesssim x \lesssim 0.45$ with $\leq 10\%$ uncertainty, which is shown in Fig. 4.

- [1] A. Accardi *et al.*, Eur. Phys. J. A **52**, 268 (2016), arXiv:1212.1701 [nucl-ex].
- [2] R. Abdul Khalek *et al.*, (2021), arXiv:2103.05419 [physics.ins-det].
- [3] X. Ji, Phys. Rev. Lett. **110**, 262002 (2013), arXiv:1305.1539 [hep-ph].
- [4] X. Ji, Sci. China Phys. Mech. Astron. **57**, 1407 (2014), arXiv:1404.6680 [hep-ph].
- [5] X. Ji, Y.-S. Liu, Y. Liu, J.-H. Zhang, and Y. Zhao, Rev. Mod. Phys. **93**, 035005 (2021), arXiv:2004.03543 [hep-ph].
- [6] M. Constantinou *et al.*, Prog. Part. Nucl. Phys. **121**, 103908 (2021), arXiv:2006.08636 [hep-ph].
- [7] K.-F. Liu and S.-J. Dong, Phys. Rev. Lett. **72**, 1790 (1994), arXiv:hep-ph/9306299.
- [8] W. Detmold and C. J. D. Lin, Phys. Rev. D **73**, 014501 (2006), arXiv:hep-lat/0507007.
- [9] V. Braun and D. Müller, Eur. Phys. J. C **55**, 349 (2008), arXiv:0709.1348 [hep-ph].
- [10] A. J. Chambers, R. Horsley, Y. Nakamura, H. Perlt, P. E. L. Rakow, G. Schierholz, A. Schiller, K. Somfleth, R. D. Young, and J. M. Zanotti, Phys. Rev. Lett. **118**, 242001 (2017), arXiv:1703.01153 [hep-lat].
- [11] A. V. Radyushkin, Phys. Rev. D **96**, 034025 (2017), arXiv:1705.01488 [hep-ph].
- [12] K. Orginos, A. Radyushkin, J. Karpie, and S. Zafeiropoulos, Phys. Rev. D **96**, 094503 (2017), arXiv:1706.05373 [hep-ph].
- [13] Y.-Q. Ma and J.-W. Qiu, Phys. Rev. Lett. **120**, 022003 (2018), arXiv:1709.03018 [hep-ph].
- [14] M. Constantinou and H. Panagopoulos, Phys. Rev. D **96**, 054506 (2017), arXiv:1705.11193 [hep-lat].
- [15] C. Alexandrou, K. Cichy, M. Constantinou, K. Hadjiyiannakou, K. Jansen, H. Panagopoulos, and F. Steffens, Nucl. Phys. B **923**, 394 (2017), arXiv:1706.00265 [hep-lat].
- [16] J.-W. Chen, T. Ishikawa, L. Jin, H.-W. Lin, Y.-B. Yang, J.-H. Zhang, and Y. Zhao, Phys. Rev. D **97**, 014505 (2018), arXiv:1706.01295 [hep-lat].
- [17] I. W. Stewart and Y. Zhao, Phys. Rev. D **97**, 054512 (2018), arXiv:1709.04933 [hep-ph].
- [18] J. R. Green, K. Jansen, and F. Steffens, Phys. Rev. D **101**, 074509 (2020), arXiv:2002.09408 [hep-lat].
- [19] X. Ji, Y. Liu, A. Schäfer, W. Wang, Y.-B. Yang, J.-H. Zhang, and Y. Zhao, Nucl. Phys. B **964**, 115311 (2021), arXiv:2008.03886 [hep-ph].
- [20] L.-B. Chen, W. Wang, and R. Zhu, Phys. Rev. Lett. **126**, 072002 (2021), arXiv:2006.14825 [hep-ph].
- [21] Z.-Y. Li, Y.-Q. Ma, and J.-W. Qiu, Phys. Rev. Lett. **126**, 072001 (2021), arXiv:2006.12370 [hep-ph].
- [22] C. Alexandrou, K. Cichy, M. Constantinou, K. Hadjiyiannakou, K. Jansen, A. Scapellato, and F. Steffens, Phys. Rev. D **99**, 114504 (2019), arXiv:1902.00587 [hep-lat].
- [23] V. M. Braun, A. Vladimirov, and J.-H. Zhang, Phys. Rev. D **99**, 014013 (2019), arXiv:1810.00048 [hep-ph].
- [24] Z. Fan, X. Gao, R. Li, H.-W. Lin, N. Karthik, S. Mukherjee, P. Petreczky, S. Syritsyn, Y.-B. Yang, and R. Zhang, Phys. Rev. D **102**, 074504 (2020), arXiv:2005.12015 [hep-lat].
- [25] X. Gao, L. Jin, C. Kallidonis, N. Karthik, S. Mukherjee, P. Petreczky, C. Shugert, S. Syritsyn, and Y. Zhao, Phys. Rev. D **102**, 094513 (2020), arXiv:2007.06590 [hep-lat].
- [26] Y.-K. Huo *et al.* (Lattice Parton Collaboration (LPC)), Nucl. Phys. B **969**, 115443 (2021), arXiv:2103.02965 [hep-lat].
- [27] J.-H. Zhang, J.-W. Chen, L. Jin, H.-W. Lin, A. Schäfer, and Y. Zhao, Phys. Rev. D **100**, 034505 (2019), arXiv:1804.01483 [hep-lat].
- [28] R. S. Sufian, J. Karpie, C. Egerer, K. Orginos, J.-W. Qiu, and D. G. Richards, Phys. Rev. D **99**, 074507 (2019), arXiv:1901.03921 [hep-lat].
- [29] T. Izubuchi, L. Jin, C. Kallidonis, N. Karthik, S. Mukherjee, P. Petreczky, C. Shugert, and S. Syritsyn, Phys. Rev. D **100**, 034516 (2019), arXiv:1905.06349 [hep-lat].
- [30] B. Joó, J. Karpie, K. Orginos, A. V. Radyushkin, D. G. Richards, R. S. Sufian, and S. Zafeiropoulos, Phys. Rev. D **100**, 114512 (2019), arXiv:1909.08517 [hep-lat].
- [31] R. S. Sufian, C. Egerer, J. Karpie, R. G. Edwards, B. Joó, Y.-Q. Ma, K. Orginos, J.-W. Qiu, and D. G. Richards, Phys. Rev. D **102**, 054508 (2020), arXiv:2001.04960 [hep-lat].
- [32] H.-W. Lin, J.-W. Chen, Z. Fan, J.-H. Zhang, and R. Zhang, Phys. Rev. D **103**, 014516 (2021), arXiv:2003.14128 [hep-lat].
- [33] X. Gao, K. Lee, S. Mukherjee, C. Shugert, and Y. Zhao, Phys. Rev. D **103**, 094504 (2021), arXiv:2102.01101 [hep-ph].
- [34] M. Gluck, E. Reya, and A. Vogt, Z. Phys. C **53**, 651 (1992).
- [35] I. Novikov *et al.*, Phys. Rev. D **102**, 014040 (2020), arXiv:2002.02902 [hep-ph].
- [36] P. C. Barry, C.-R. Ji, N. Sato, and W. Melnitchouk (Jefferson Lab Angular Momentum (JAM)), Phys. Rev. Lett. **127**, 232001 (2021), arXiv:2108.05822 [hep-ph].
- [37] M. Aicher, A. Schafer, and W. Vogelsang, Phys. Rev. Lett. **105**, 252003 (2010), arXiv:1009.2481 [hep-ph].
- [38] A. Bazavov *et al.* (HotQCD), Phys. Rev. D **90**, 094503 (2014), arXiv:1407.6387 [hep-lat].
- [39] E. Follana, Q. Mason, C. Davies, K. Hornbostel, G. P. Lepage, J. Shigemitsu, H. Trotter, and K. Wong (HPQCD, UKQCD), Phys. Rev. D **75**, 054502 (2007), arXiv:hep-lat/0610092.
- [40] A. Hasenfratz and F. Knechtli, Phys. Rev. D **64**, 034504 (2001), arXiv:hep-lat/0103029.
- [41] X. Ji, J.-H. Zhang, and Y. Zhao, Phys. Rev. Lett. **120**, 112001 (2018), arXiv:1706.08962 [hep-ph].
- [42] T. Ishikawa, Y.-Q. Ma, J.-W. Qiu, and S. Yoshida, Phys. Rev. D **96**, 094019 (2017), arXiv:1707.03107 [hep-ph].
- [43] J. Green, K. Jansen, and F. Steffens, Phys. Rev. Lett. **121**, 022004 (2018), arXiv:1707.07152 [hep-lat].
- [44] C. Bauer, G. S. Bali, and A. Pineda, Phys. Rev. Lett. **108**, 242002 (2012), arXiv:1111.3946 [hep-ph].
- [45] J.-H. Zhang, J.-W. Chen, X. Ji, L. Jin, and H.-W. Lin, Phys. Rev. D **95**, 094514 (2017), arXiv:1702.00008 [hep-lat].
- [46] C. Alexandrou, K. Cichy, M. Constantinou, J. R. Green, K. Hadjiyiannakou, K. Jansen, F. Manigrasso, A. Scapellato, and F. Steffens, Phys. Rev. D **103**, 094512 (2021), arXiv:2011.00964 [hep-lat].
- [47] A. Bazavov, P. Petreczky, and J. H. Weber, Phys. Rev. D **97**, 014510 (2018), arXiv:1710.05024 [hep-lat].

- [48] A. Bazavov, N. Brambilla, H. T. Ding, P. Petreczky, H. P. Schadler, A. Vairo, and J. H. Weber, *Phys. Rev. D* **93**, 114502 (2016), arXiv:1603.06637 [hep-lat].
- [49] A. Bazavov, N. Brambilla, P. Petreczky, A. Vairo, and J. H. Weber (TUMQCD), *Phys. Rev. D* **98**, 054511 (2018), arXiv:1804.10600 [hep-lat].
- [50] T. Izubuchi, X. Ji, L. Jin, I. W. Stewart, and Y. Zhao, *Phys. Rev. D* **98**, 056004 (2018), arXiv:1801.03917 [hep-ph].
- [51] M. Burkardt, J. M. Grandy, and J. W. Negele, *Annals Phys.* **238**, 441 (1995), arXiv:hep-lat/9406009.
- [52] M. Beneke and V. M. Braun, *Nucl. Phys. B* **426**, 301 (1994), arXiv:hep-ph/9402364.
- [53] X. Xiong, X. Ji, J.-H. Zhang, and Y. Zhao, *Phys. Rev. D* **90**, 014051 (2014), arXiv:1310.7471 [hep-ph].
- [54] Y.-Q. Ma and J.-W. Qiu, *Phys. Rev. D* **98**, 074021 (2018), arXiv:1404.6860 [hep-ph].
- [55] Y. Zhao *et al.*, “in preparation.”
- [56] P. Petreczky and S. Steinbeißer (2021) arXiv:2112.00788 [hep-lat].
- [57] V. M. Braun, K. G. Chetyrkin, and B. A. Kniehl, *JHEP* **07**, 161 (2020), arXiv:2004.01043 [hep-ph].
- [58] G. S. Bali, C. Bauer, A. Pineda, and C. Torrero, *Phys. Rev. D* **87**, 094517 (2013), arXiv:1303.3279 [hep-lat].
- [59] G. S. Bali, C. Bauer, and A. Pineda, *Phys. Rev. D* **89**, 054505 (2014), arXiv:1401.7999 [hep-ph].
- [60] G. S. Bali, C. Bauer, and A. Pineda, *Phys. Rev. Lett.* **113**, 092001 (2014), arXiv:1403.6477 [hep-ph].
- [61] G. S. Bali, S. Collins, B. Gläbke, M. Göckeler, J. Najjar, R. H. Rödl, A. Schäfer, R. W. Schiel, A. Sternbeck, and W. Söldner, *Phys. Rev. D* **90**, 074510 (2014), arXiv:1408.6850 [hep-lat].
- [62] A. Pineda, *J. Phys. G* **29**, 371 (2003), arXiv:hep-ph/0208031.
- [63] M. A. Shifman, A. I. Vainshtein, and V. I. Zakharov, *Nucl. Phys. B* **147**, 385 (1979).
- [64] M. A. Shifman, A. I. Vainshtein, and V. I. Zakharov, *Nucl. Phys. B* **147**, 448 (1979).
- [65] V. A. Novikov, M. A. Shifman, A. I. Vainshtein, and V. I. Zakharov, *Phys. Rept.* **116**, 103 (1984).
- [66] V. A. Novikov, M. A. Shifman, A. I. Vainshtein, and V. I. Zakharov, *Nucl. Phys. B* **249**, 445 (1985).
- [67] F. David, *Nucl. Phys. B* **263**, 637 (1986).
- [68] P. Petreczky and J. H. Weber, (2020), arXiv:2012.06193 [hep-lat].
- [69] A. F. Falk, H. Georgi, B. Grinstein, and M. B. Wise, *Nucl. Phys. B* **343**, 1 (1990).
- [70] G. Curci, W. Furmanski, and R. Petronzio, *Nucl. Phys. B* **175**, 27 (1980).